NUMERICAL STUDY OF MAGNETOHYDRODYNAMICS AND MIXED CONVECTION CHARACTERISTICS OF AN ELECTRICALLY CONDUCTING FLUID

Prithvi Ramesh

NUMERICAL STUDY OF MAGNETOHYDRODYNAMICS AND MIXED CONVECTION CHARACTERISTICS OF AN ELECTRICALLY CONDUCTING FLUID

Thesis report submitted to
BITS-Pilani Goa
as part for the award of the degree

of

Bachelor of Technology

by

Prithvi Ramesh

Under the guidance of

Prof. Manab Kumar Das

IIT Kharagpur

BITS Pilani
K K Birla Goa Campus

DEPARTMENT OF MECHANICAL ENGINEERING

BITS PILANI GOA

CERTIFICATE

This is to certify that the report entitled, **Numerical Study of Magnetohydrodynamics and Mixed Convection Characteristics of an Electrically Conducting Fluid** , submitted by **Prithvi Ramesh** to BITS-Pilani Goa is a record of bona fide thesis work under my supervision.

Dr. Manab Kumar Das

Professor

Mechanical Engineering

Department

Indian Institute of Technology

Kharagpur, 721302

DECLARATION

I certify that

1. The work contained in the thesis is original and has been done by myself under the general supervision of my supervisor(s).

2. The work has not been submitted to any other Institute for any degree or diploma.

3. I have followed the guidelines provided by the Institute in writing the thesis.

4. I have conformed to the norms and guidelines given in the Ethical Code of Conduct of the Institute.

5. Whenever I have used materials (data, theoretical analysis, and text) from other sources, I have given due credit to them by citing them in the text of the thesis and giving their details in the references.

6. Whenever I have quoted written materials from other sources, I have put them under quotation marks and given due credit to the sources by citing them and giving required details in the references.

Contents

List of Figures

ABSTRACT

Magnetohydrodynamics is the study of the motion of electrically conducting fluids in the presence of an external homogeneous magnetic field. These fluids experience a force called the Lorentz force which significantly alters the velocity field. Four variations are considered with the Stuart numbers of 0,1,10 and 50. The analysis is extended to a shear-thinning and shear-thickening non-Newtonian fluids. The analysis revealed that the central core vortex is split into multiple vortices upon the application of the external magnetic field which also weakens the strength of the core vortex. The influence of the magnetic field was found to be more profound for the shear-thinning fluid and less for the shear-thickening. Three types of convective heat transfer were also investigated - forced convection , natural convection and mixed convection and the solvers created to to analyse them were validated using published data. The study is further extended for turbulent flows using the K-Epsilon turbulence model and both magnetohydrodynamics and mixed convection are considered.

x

Magnetohydrodynamic effects

1.1 Introduction

Electrically conducting fluids experience a force when an external magnetic field is applied on them. This external force is modeled using Maxwell's equations of electrostatics and is included as a body force in the Naiver-Stokes equations. The effect of the force on fluids is investigated for four different Stuart's numbers namely -0, 5, 10, 50 with the Reynolds number kept constant at 100. Non-Newtonian fluids do not follow the Newton's law of linear variance of stress to the rate of shear strain, the viscosity of these fluids depends on the force applied, while for Newtonian fluids the viscosity remains constant. The Power-law scheme is used to model the Non-Newtonian behavior with the power-law coefficient taken as 0.6 and 1(for Newtonian). The case is setup for a lid-driven cavity, in which the flow is driven by the upper wall. The walls are assumed to be perfectly non-conducting. The standard OpenFOAM solver-mhdfoam is modified to model the viscosity with the power-law scheme. This study finds applications in healthcare and metallurgical industries. Since blood flow in an Magnetic Resonance Imaging(MRI) instrument is modeled as a Non-Newtonian MHD fluid under the influence of an external magnetic field. The validation is done using the results published in Kefayati (2014). It has been inferred that the deviation of Non-Newtonian from Newtonian behavior is increased with increase in Stuart Number. Furthermore the external magnetic field lines split the fluid flow into two or more vortices as the Stuart Number increases.

1.1.1   Governing Equations

A moving stream of an electrically under the influence of an externally imposed magnetic field experiences Lorentz force. These Lorentz forces oppose the motion of the fluid in a direction perpendicular to the field lines. The currents themselves induced a secondary field which according to Faraday's law oppose the external field. Therefore the sum of the external field (Bo) and the induced field (b) is the total magnetic field.

$$Bo = B + b \tag{1.1}$$

The four Maxwell's equations used in conjunction with Naiver-Stokes equations are:

1. Gauss's law of Electrostatics

The divergence of the electric field developed depends on the charge density ρ_c and the permittivity of free space ϵ_o

$$\nabla . E = \frac{\rho_c}{\epsilon_0} \tag{1.2}$$

2. Gauss's law of Magnetism

Gauss's law of magnetism dictates that magnetic field lines behave like streamlines of incompressible fluids- there cannot be an isolated North or South poles. B- magnetic field

$$\nabla . B = 0 \tag{1.3}$$

3. Faraday's Law
Time change in mangetic fields can create electric fields.

$$\nabla \times E = -\frac{\partial B}{\partial t} \tag{1.4}$$

4.Amphere-Maxwell's Law

Time change in electric fields can create an induced magnetic field.μ_o- magnetic permitivity of free space , c - speed of light

$$\nabla \times B = \mu_0 J + \frac{1}{c^2}\frac{\partial E}{\partial t} \tag{1.5}$$

The Lorentz force which combines the effect of electric and magnetic fields for a fluid particle is given as:

$$F = q\overrightarrow{E} + q(\vec{V} \times \overrightarrow{B}) \tag{1.6}$$

The same equation is expressed in the volumetric form based on the continuum hypothesis (dividing by a infinitesimal volume)

$$f = \rho_c\overrightarrow{E} + \rho_c(\vec{V} \times \overrightarrow{B})$$

The velocity component in the above equation is combined with charge density to form the current density- $\overrightarrow{J}$

$$f = \rho_c\overrightarrow{E} + (\vec{J} \times \overrightarrow{B}) \tag{1.7}$$

The following assumptions are involved in the Ideal MHD formulation-

1. The effect of the electric fields are negligible

2. The induced magnetic field has a negligible effect

3. The fluid velocity and the charge velocity are the same- allowing for the coupling of the Naiver-Stokes and Maxwell's equations

By neglecting electric field, (Eq. 1.6) becomes,

$$f = J \times B \tag{1.8}$$

The coupled Naiver-Stokes and Maxwell's equations(Eq. 1.2) with the Lorentz force added as a body force is given as:

$$\rho(D\overrightarrow{V}/Dt) = -\nabla p + \mu\nabla^2\overrightarrow{V} + \overrightarrow{J} \times \overrightarrow{B} \tag{1.9}$$

since, the magnetic field lines $\overrightarrow{B}$ can be written as(Amphere-Maxwell Law (Eq..1.5)
:

$$\nabla \times \overrightarrow{B} = \mu_o \overrightarrow{J} \tag{1.10}$$

Using vector identity,

$$\nabla \times F \times G = F(\nabla.G) - G(\nabla.F) + (G.\nabla)F - (F.\nabla)G \tag{1.11}$$

The coupled Naiver-Stokes and Maxwell's equation is :

$$\rho(D\overrightarrow{V}/Dt) = -\nabla p + \mu \nabla^2 \overrightarrow{V} + ((\overrightarrow{B}.\nabla)\overrightarrow{B}/\mu_o) - (\nabla B^2/(2*\mu_o)) \tag{1.12}$$

where,

$$((\overrightarrow{B}.\nabla)\overrightarrow{B}/\mu_o)\text{-Magnetic pressure (scalar)}$$

$$\nabla B^2/(2*\mu_o)\text{-Magnetic Tension (in the fluid flow direction)}$$

The magnetic field lines - $\overrightarrow{B}$ can be visualized as the velocity field $\overrightarrow{V}$, therefore the $\overrightarrow{B}$ can be treated as an additional variable like the velocity to be solved for. Further a transport equation called the induction equation and a corrector equation are required to close the set of equations.

The current density is given as (By Ohm's Law):

$$j = \sigma E^* \tag{1.13}$$

where E^* is the electric field in a frame of reference fixed to the material. If the conductor moves with a velocity v,

$$E^* = E + v \times B \tag{1.14}$$

The current density in a moving conductor is given by Ohm's law

$$j = \sigma E^* = \sigma (E + v \times B) \tag{1.15}$$

- Apply curl operator on Ohm's law for moving fluids (Eq. 1.21)

- Substitute the electric field (Eq.) and the current density (Eq. 1.5)

- B is solenoidal i.e. $\nabla.B = 0$ (Eq. 1.3)

- Flow is incompressible i.e. $\nabla.V = 0$

- Vector analytical rearrangement

$$\partial \vec{B}/\partial t = \eta \nabla^2 \vec{B} + \nabla \times (\vec{V} \times \vec{B}) \tag{1.16}$$

Magnetic Transport Equation-

$$\partial \vec{B}/\partial t = \eta \nabla^2 \vec{B} + \nabla \times (\vec{V} \times \vec{B}) \tag{1.17}$$

Magnetic Continuity Equation-

$$\nabla.B \overset{\rightarrow}{=} 0 \tag{1.18}$$

The velocity needs to be known for these equations to be solved, therefore a second algorithm called the 'BPISO' algorithm is used to solve for B after the velocity is known from the PISO algorithm

The four governing equations are:

$$\rho(D\vec{V}/Dt) = -\nabla p + \mu \nabla^2 \vec{V} + ((\vec{B}.\nabla)\vec{B}/\mu_o) - (\nabla B^2/(2 * \mu_o)) \tag{1.19}$$

$$\nabla.\vec{V} = 0 \tag{1.20}$$

$$\partial \vec{B}/\partial t = \eta \nabla^2 \vec{B} + \nabla \times (\vec{V} \times \vec{B}) \tag{1.21}$$

$$\nabla.B \overset{\rightarrow}{=} 0 \tag{1.22}$$

The OpenFOAM solver utilizes a second PISO loop for calculating the magnetic field - BPISO. The pressure analog of BPSIO is the scalar fictitious magnetic field-pB which is used to initiate the loop. Figure(1) shows the governing equations and the scalar values used in the solver.

$$\frac{\partial \mathbf{B}}{\partial t} + \nabla \bullet (\mathbf{VB}) - \nabla \bullet (\mathbf{BV}) - \Delta \left(\frac{1}{\mu_0 \sigma}\mathbf{B}\right) = 0$$

(a) Governing Equations in the OpenFOAM Solver

```
#include "CourantNo.H"

{
fvVectorMatrix UEqn
(
fvm::ddt(U)
+ fvm::div(phi, U)
- fvc::div(phiB, 2.0*DBU*B)
- fvm::laplacian(nu, U)
+ fvc::grad(DBU*magSqr(B))
);

if (piso.momentumPredictor())
{
solve(UEqn == -fvc::grad(p));
}
```

(b) Momentum Transport Equation

```
dimensionedScalar DB = 1.0/(mu*sigma);
DB.name() = "DB";

dimensionedScalar DBU = 1.0/(2.0*mu*rho);
DBU.name() = "DBU";
```

(c) Dimensionless Scalars

Figure 1.1:

1.1.2 Fluid Model

The Non-Newtonian Power Law scheme is used to define the viscosity of the fluid with the strain rate as follows:

$$\vartheta = K\gamma^{n-1} \tag{1.23}$$

where,

K- Consistency Coefficient

γ - Intensity of Strain Rate

n - Power-law index

The values of n used in this study is 1 (Newtonian) and 0.6 (Non-Newtonian) . The value of $n < 1$ defines a shear-thinning fluid in which the fluid's viscosity decreases as it is subjected to shearing force.

1.2   Problem Definition and Case Setup

1.2.1   Computational Domain and Non-dimensional Parameters

The computational domain consists of a square cavity with the upper wall given a shearing motion. The dimensions of the computational domain are 0.1 m by 0.1 m by 0.01m.

	Pressure	Velocity	Magnetic Field(Tesla)	pB
Top Wall	zeroGradient	(V,0,0)	zeroGradient	0
Bottom Wall	ZeroGradient	(-V,0,0)	zeroGradient	0
Fixed (side) Walls	zeroGradient	noSlip	zeroGradient	0

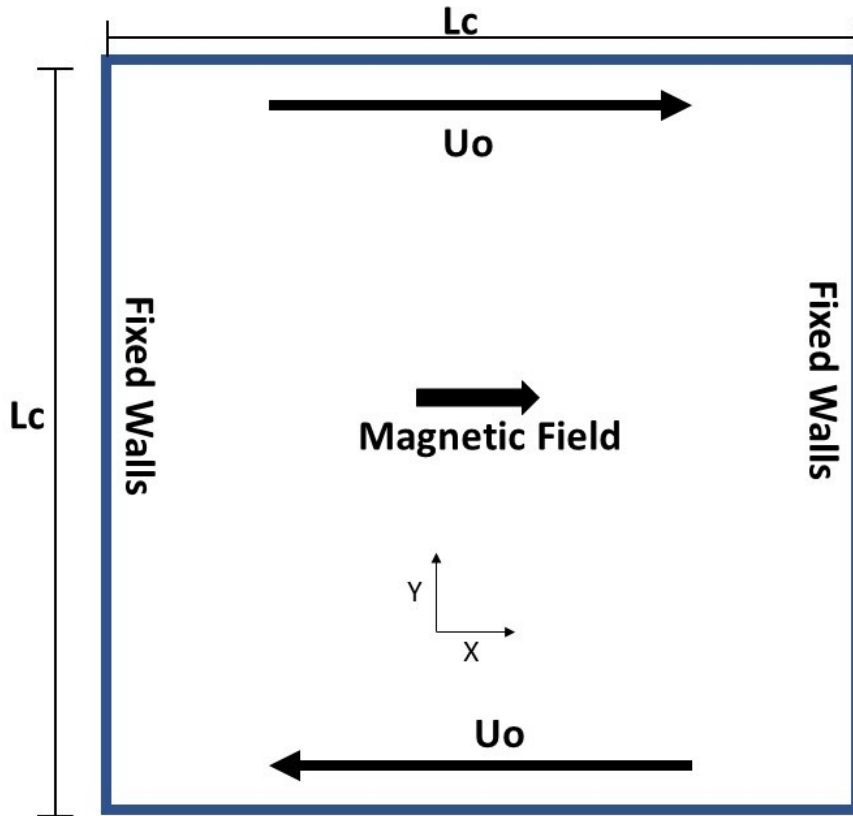Figure 1.2: Boundary Conditions

Figure 1.3: Computational domain

Uniform homogeneous external magnetic field is applied in the domain in the positive 'x' direction. The walls are assumed to be perfectly conducting and the flow is assumed to be incompressible and induction-less.

The following dimensionless parameters are used in the study:

1. Hartmann Number (Ha) which is expressed as a ratio of the electromagnetic force and the viscous forces.

$$B\left(\frac{L_c^{n+1}\sigma}{V_c^{n-1}K}\right)^{1/2} \tag{1.24}$$

2. Reynolds Number (Re) which is expressed as the ratio of inertial force to the viscous force

$$\left(\frac{\rho V_c^{2-n}L_c^n}{K}\right) \tag{1.25}$$

3. Stuart Number which is expressed as the ratio of electromagnetic force to the inertia force

$$\left(\frac{Ha^2}{Re}\right) \tag{1.26}$$

where σ is the conductivity of the fluid, L_c is the characteristic length of the cavity, V_c the velocity of thee upper wall K consistency coefficient

1.2.2   Case Setup

The computational grid consists of a 200x200 number of cells with the size of the grid cells reduced near the walls too capture the near-wall gradients.
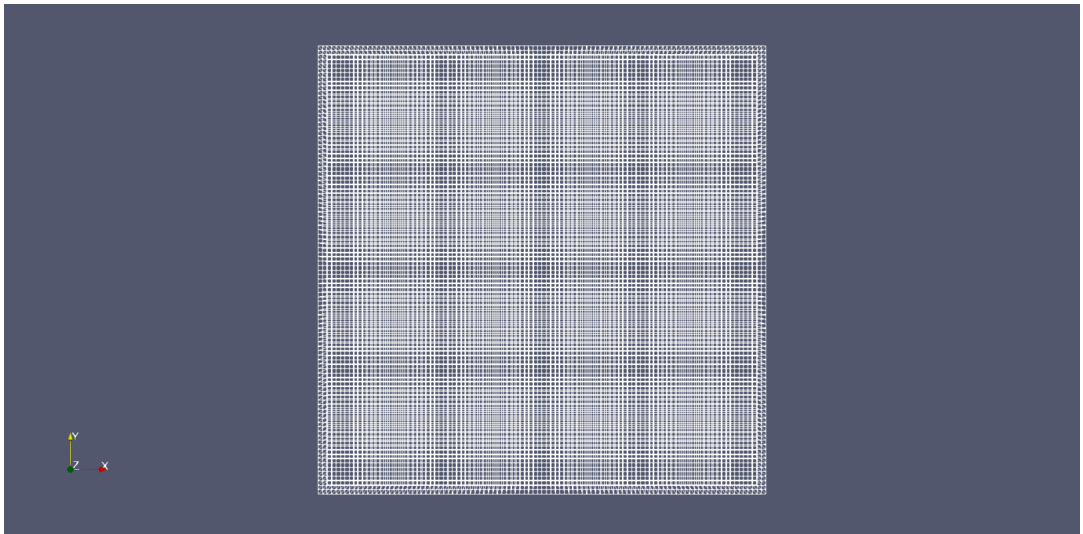

Figure 1.4: Computational Grid

The fluid properties are given below in the table:

Property	Property Value	SI units
Density	1060	kg/m^3
Consistency Coefficient	0.004	kg/ms
Maximum Dynamic Viscosity	0.01	kg/ms
Minimum Dynamic Viscosity	0.001	kg/ms
Power Law Index	1-Newtonian , 0.6-Non-Newtonian	
Electrical Conductivity	0.625	S/m
Magnetic Constant	1.257E-06	H/m

Figure 1.5: Fluid Properties

The values of the uniform magnetic field is calculated for each of the eight cases based on the Stuart number and the values of the characteristic length and the fluid properties.

Stuart Number	Newtonian(n=1)	Non-Newtonian(n=0.6)
0	(0,0,0)	(0,0,0)
5	(8 0 0)	(12.77647 0 0)
10	(25.29822 0 0)	(40.40274 0 0)
50	(56.56854 0 0)	(90.34328 0 0)

Figure 1.6: Values of Magnetic Field

Reynolds number has been kept constant at 100 for thee study and further the velocity magnitude has been taken as 0.003773585 m/s for Newtonian and 0.009624891 for Non-Newtonian. The time step is taken as 0.005s and all cases are run to 350 seconds.

1.3   Results and Discussion

The validation is carried out for non-Newtonian fluid with a power-law index of 0.6 and Reynolds number of 100 with data published in Kefayati(2014)[9].The graphs plotted are along the cavity height (y-axis) and the values of the x-component of velocity divided by the magnitude(non-dimensional velocity)
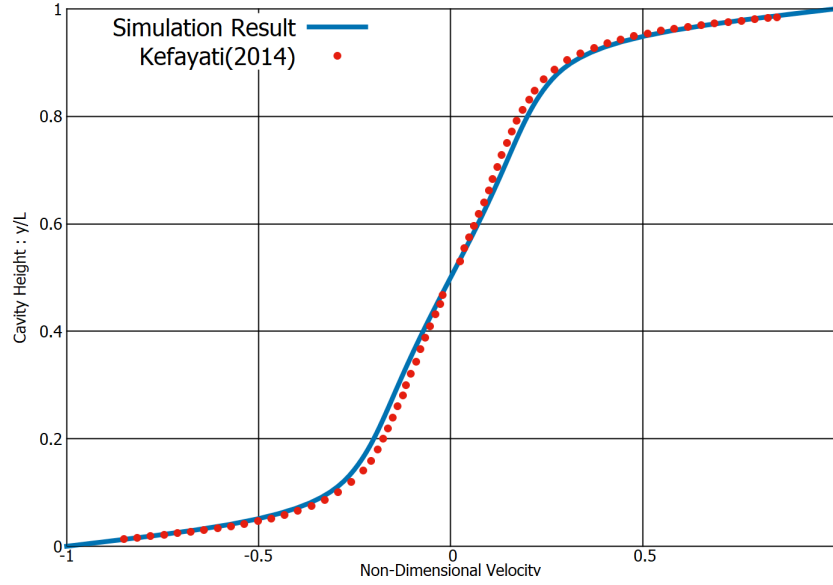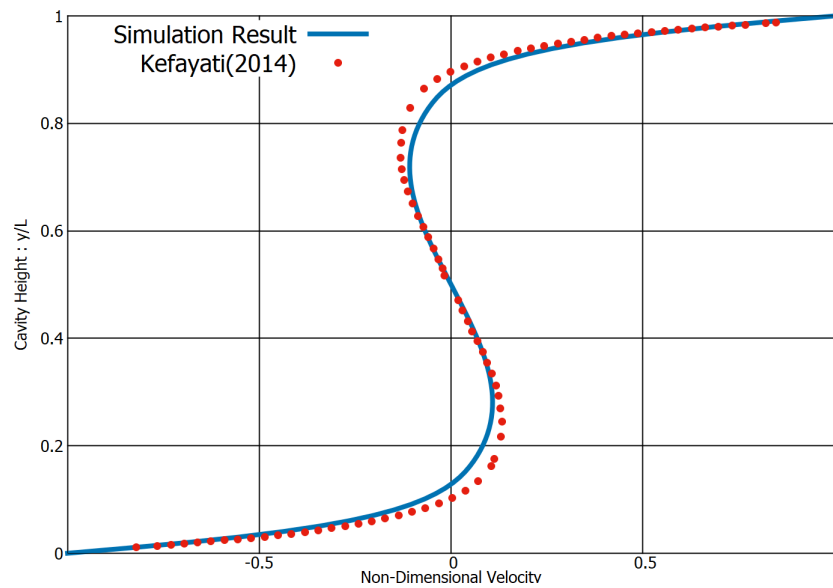

Figure 1.7: Stuart Number=0
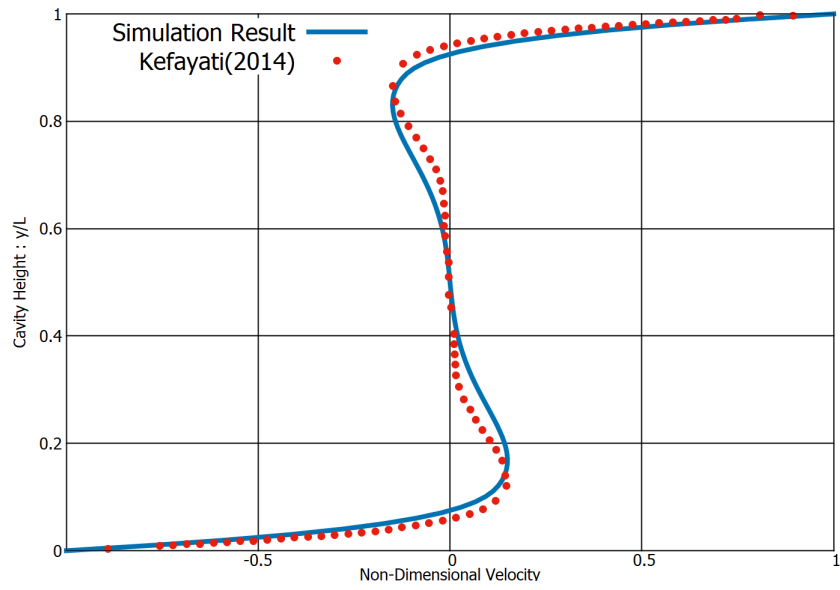

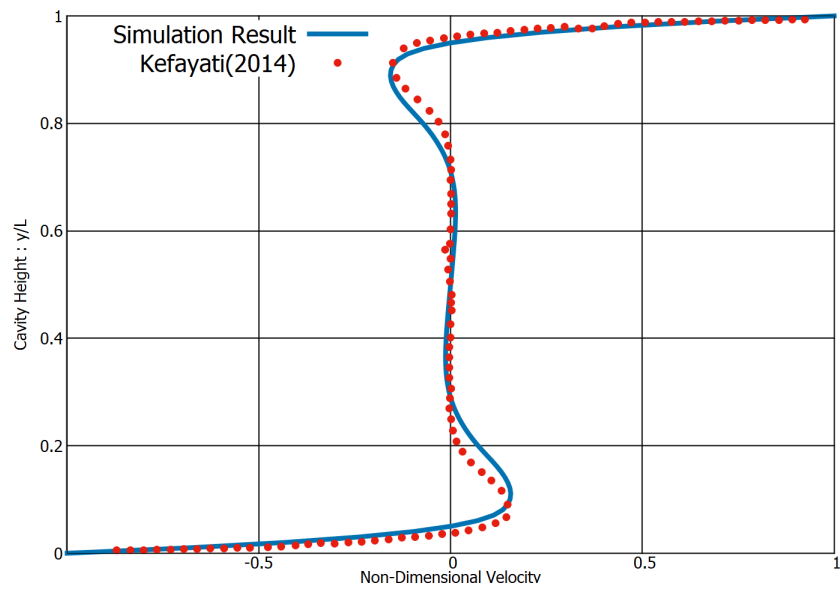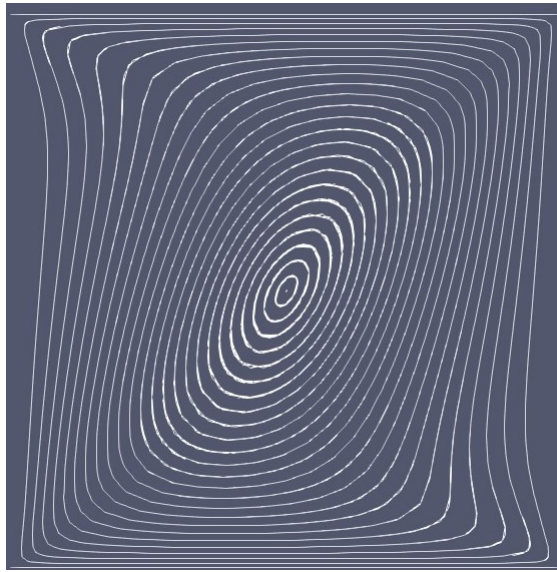Figure 1.8: Stuart Number=1

Figure 1.9: Stuart Number =10
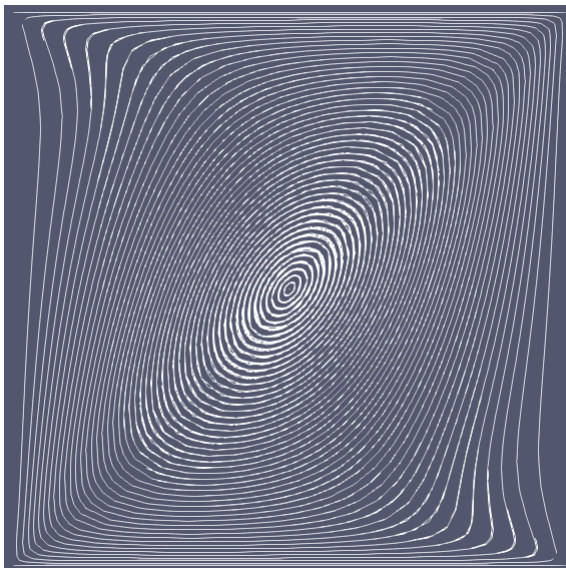

Figure 1.10: Stuart Number=50

The validation study shows that simulation data to be in close agreement with the experimental data published by Kefayati(2014)[9]

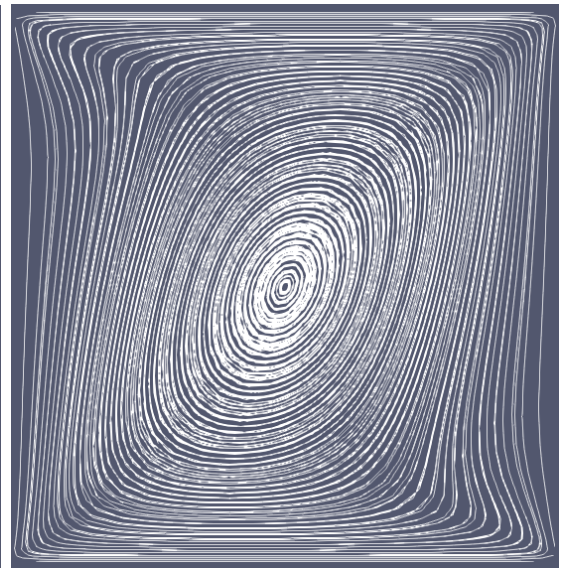## 1.3.1   Comparison of Newtonian and Non-Newtonian Results

1.3.1.1   Streamlines

(a) Newtonian
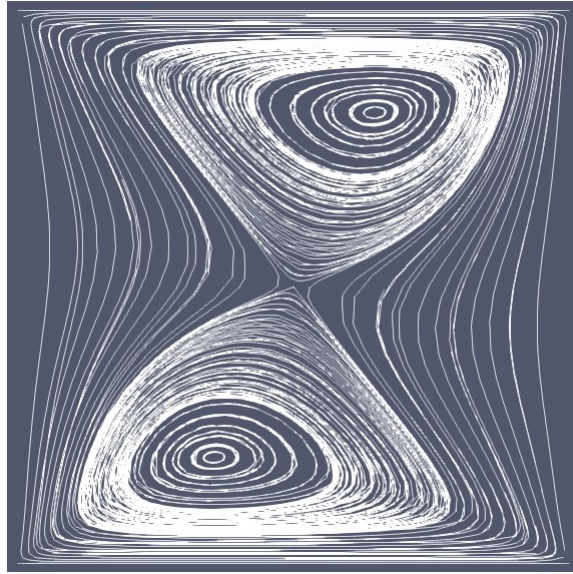

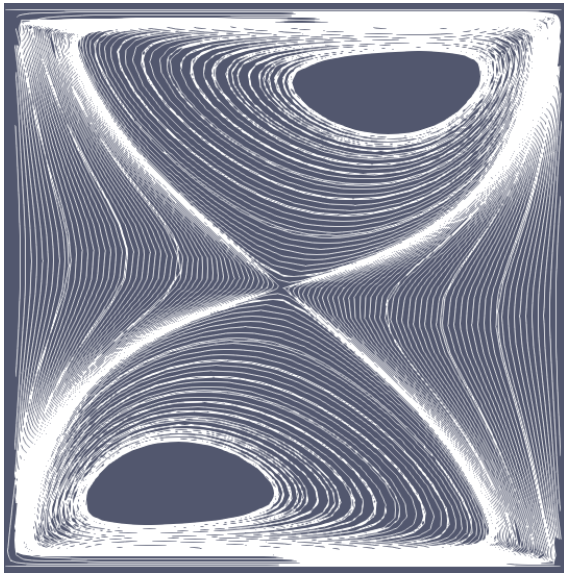(b) Shear-Thinning

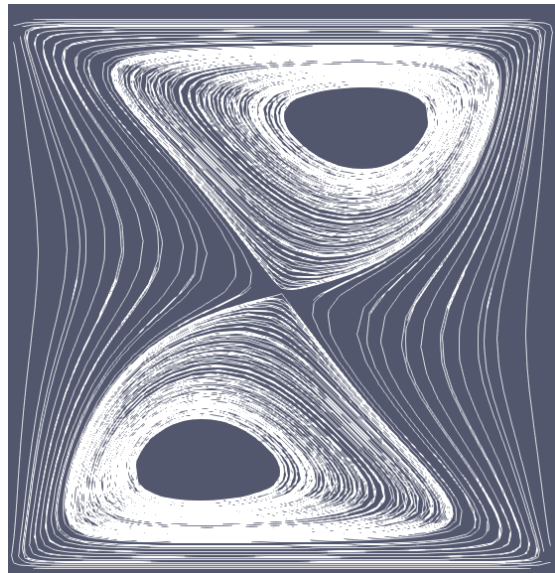(c) Shear-Thickening

Figure 1.11: Stuart number=0

(a) Newtonian

(b) Shear-Thinning

(c) Shear-Thickening

Figure 1.12: Stuart number=1

(a) Newtonian

(b) Shear-Thinning

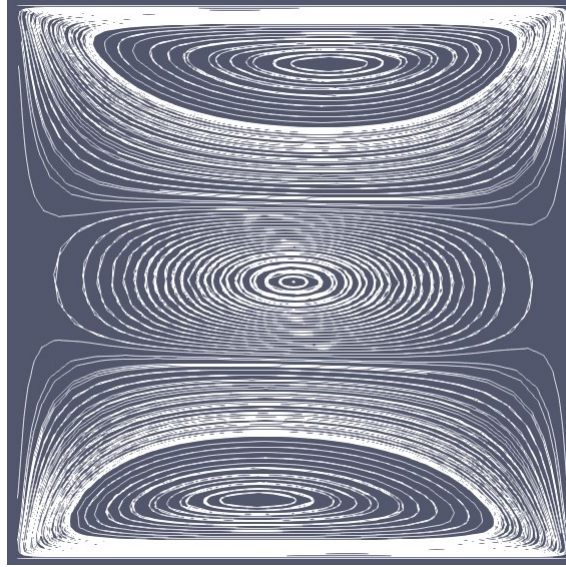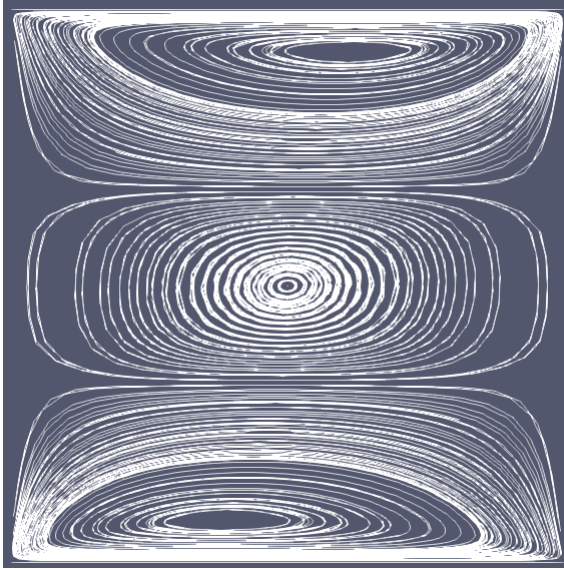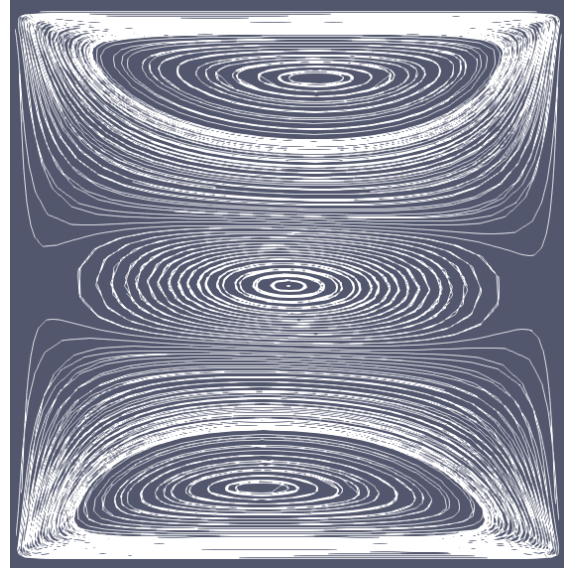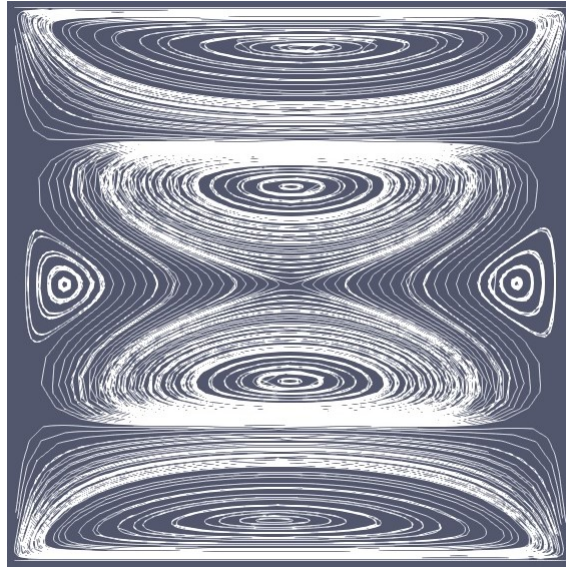(c) Shear-Thickening

Figure 1.13: Stuart number=10

(a) Newtonian
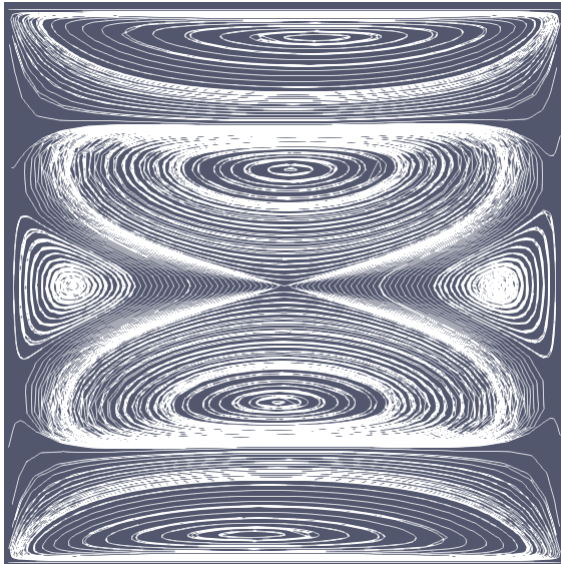
(b) Shear-Thinning
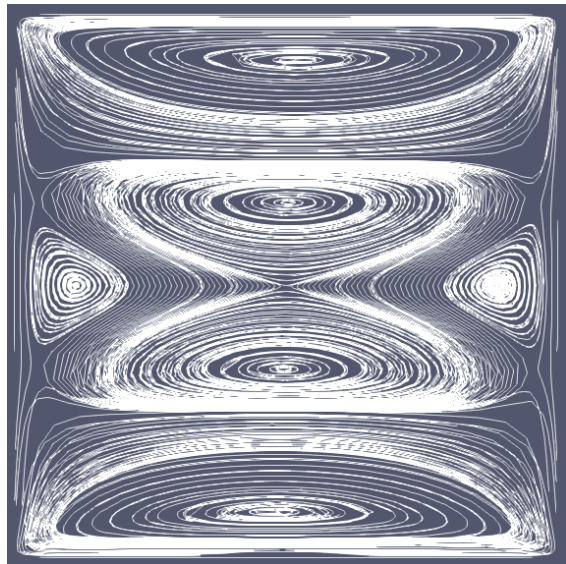
(c) Shear-Thickening

Figure 1.14: Stuart number=50

1.3.1.2   Velocity Plot Result
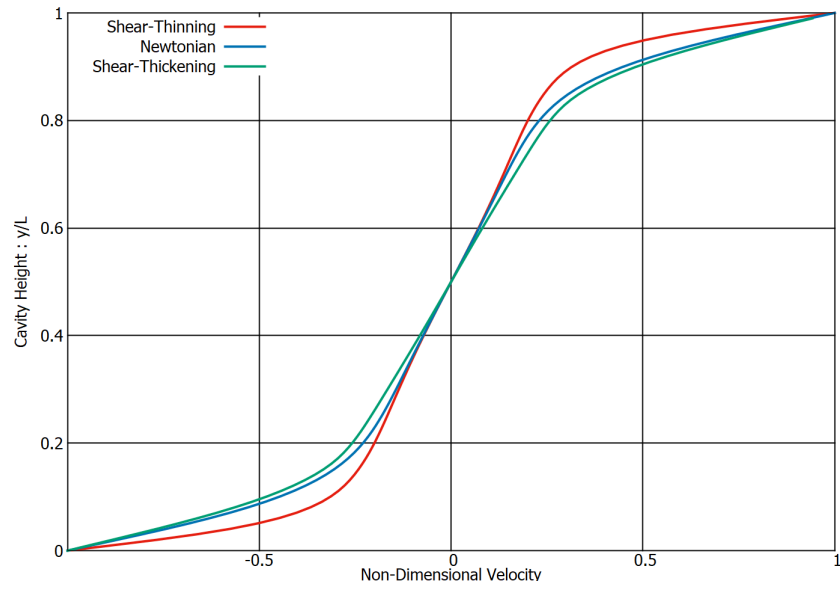
Figure 1.15: Stuart Number=0
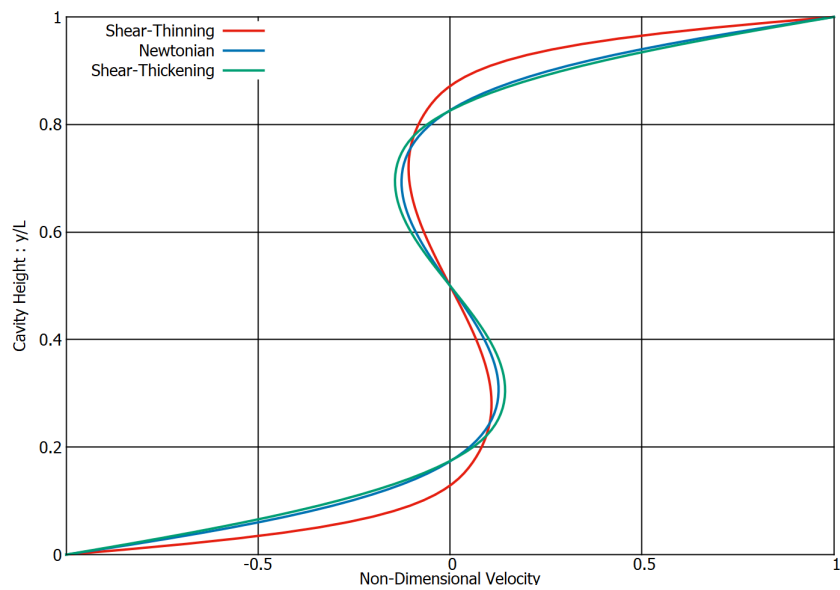
Figure 1.16: Stuart Number=1
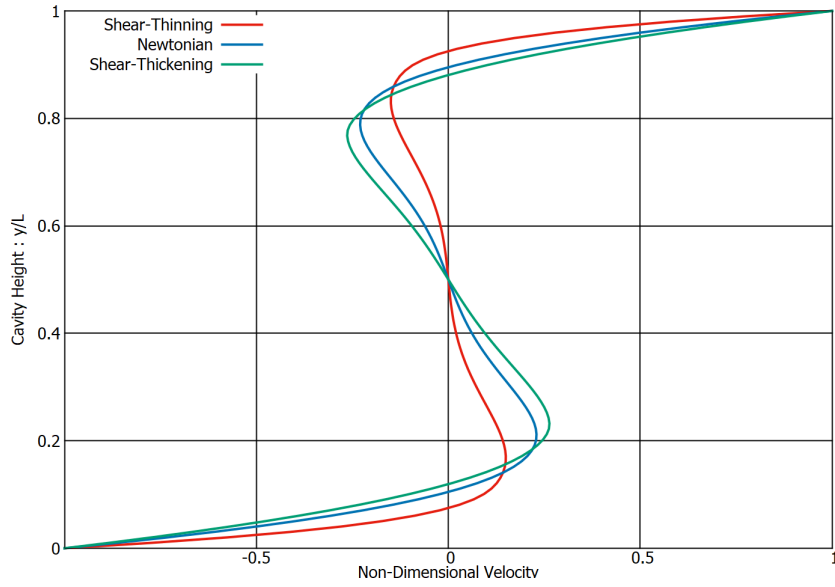
Figure 1.17: Stuart Number=10
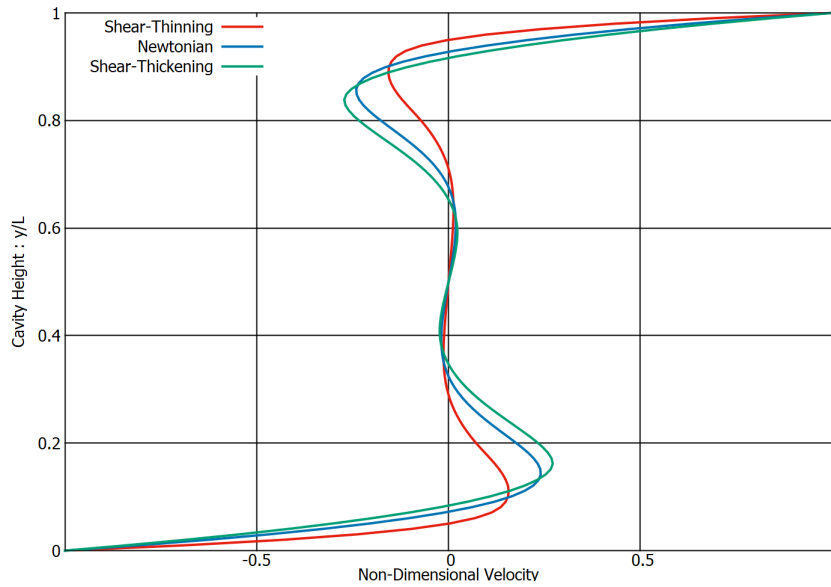
Figure 1.18: Stuart Number=50

1.4   Conclusions

The streamlines presented in Figures[1.11,1.12,1.13,1.14] show that the effect of the external magnetic field is to split the core vortex into multiple smaller vortices. The core vortex consists of a single clockwise vortex when no magnetic field is applied. For a Stuart number of 11.12, the flow splits into two clockwise vortices. The flow is split into three vortices for Stuart number=10 which consists of a central anti-clockwise vortex and two clockwise vortices at the top and bottom. The central anticlockwise vortex is further split into two anti-clockwise vortices for the Stuart number=50 , in addition, two clockwise vortices appear in the left and the right. The velocity

plot in Figures[1.7,1.8,1.9,1.10] indicate that the simulation results are in close agreement with the published data. In Figure[1.15] the velocity profile is symmetric and is positive in the top half and negative in the bottom half, further due to the symmetric nature the velocity become zero for the center of the domain. Since the core vortex is split into two for Stuart Number=1 the Figure[1.16] depicts an "S"shaped profile. The profile in Figures[1.17,1.18] has a decreased peak value of velocity magnitude(maximum distance from the zero-velocity line) due to the formation of an anti-clockwise vortex in the center. It therefore can be inferred though that the total magnitude of the velocity decreases for increased Stuart numbers since the profile is closer to the zero-velocity vertical line: this suggest that the magnetic field weakens the strength of the core vortex. A comparison of the Newtonian and non-Newtonian fluid profiles is presented in Figure[1.15,1.16,1.17,1.18] which illustrate that the decrease in the magnitude of absolute velocity for a given Stuart number is more for the shear-thinning fluid, and less for a shear-thickening. The deviation for shear-thickening is lesser than the shear-thinning since 1.2 power-law was closer to Newtonian fluid than 0.6 power-law. Therefore it can be concluded that the influence of the magnetic filed is higher for a shear-thinning fluid compared to a shear-thickening fluid.

Thermal Effects

2.1 Introduction

Convection is a form of heat transfer which is facilitated through the motion of fluid. In case of "Forced Convection" the fluid motion is due to an external force such as an upper shearing wall used in this study. When the fluid is set into motion due to body forces arsing from density difference due to different temperature- the convection currents are induced- this form of convection is termed- "Natural Convection". In this study both natural and forced convection phenomena are studied in-depth through CFD simulation of a single phase fluid in a lid-driven cavity. The reference papers used for the study are "Santos et al(2013)" for forced convection and "Wan et al (2001)"

The energy equation is a P.D.E which included thermal energy in the form of absolute temperature as a transport equation. This transport equation is solved in the study to determine the distribution of temperature throughout the fluid domain. The temperature is modeled as a scalar. The first form of temperature transport is through diffusion which is represented as the laplacian in the right hand side. The convection transport is the has the velocity vector attached with the temperature gradient as a dot product. Therefore the PISO algorithm is implemented to determine the velocity distribution in the domain before the temperature distribution is plotted. The time dependence time makes the equation a transient equation. Since the equation is perfectly linear, a pseudo temperature value is not required for making the equation linear. (unlike the non-linear Navier Stokes equation which uses "phiU").

$$\frac{\partial T}{\partial t} + V.\nabla T = \nabla^2 T \tag{2.1}$$

2.1.1   Dimensionless Parameters

The thermal diffusivity which is indicated by the symbol α is the ability of a material to transfer heat compared to its heat capacity and density. It is represented by the thermal conductivity(k) of the material divided by the product of the density(ρ)and the heat storage capacity (specific heat capacity) -C_p.

$$\alpha = \frac{k}{\rho C_p} \tag{2.2}$$

The other non-dimensional number used for forced convection study is the Prandtl's number which is the ratio of the kinematic diffusivity to the thermal diffusivity.

$$Pr = \frac{\nu}{\alpha} \tag{2.3}$$

The non-dimensional parameters used in the natural convection portion of the study are given here:

$$x = \frac{\bar{x}}{L_c}, y = \frac{\bar{y}}{L_c} \tag{2.4}$$

$$u = \frac{\bar{u}L_c}{\alpha}, v = \frac{\bar{v}L_c}{\alpha} \tag{2.5}$$

$$t = \frac{\alpha\bar{t}}{L_c^2} \tag{2.6}$$

$$p = \frac{\bar{p}L_c^2}{\rho\alpha^2} \tag{2.7}$$

$$Pr = \frac{\nu}{\alpha} \tag{2.8}$$

where, L_c is the cavity length, α is the thermal diffusivity, $\bar{x}, \bar{y}$ are dimensional coordinates, $\bar{T}$ is the dimensional temperature (in kelvin) , T_c, T_H are the dimensional extreme temperatures.

The Grashof Number is the ratio of the buoyancy forces to the viscous forces- this parameter is significant in controlling convection flow, , it is given as:

$$Gr = \frac{g\beta T L_c^3}{\vartheta^2} \tag{2.9}$$

The parameter of interest in this study is the Rayleigh number which is the product of Grashof's number and the Prandtl's number, which is given as:

$$Ra = Pr * Gr = \frac{g\beta T L_c^3}{\vartheta\alpha} \tag{2.10}$$

where ,

g is the acceleration due to gravity

β is coefficient of thermal expansion

ϑ is the kinematic viscosity

L_c is the characteristic length of the cavity

α is the thermal diffusivity

2.1.2   Governing Equations

2.1.2.1   Forced Convection

In addition to the standard Navier-Stokes equations of continuity and momentum-the energy equation is also solved for the temperature distribution.

The governing equations used for forced convection are:

$$\nabla.V = 0 \tag{2.11}$$

$$\frac{\partial u}{\partial t} + V.\nabla u = -\nabla p + Pr\nabla^2 u \tag{2.12}$$

$$\frac{\partial v}{\partial t} + V.\nabla v = -\nabla p + Pr\nabla^2 v \tag{2.13}$$

$$\frac{\partial T}{\partial t} + V.\nabla T = \nabla^2 T \tag{2.14}$$

2.1.2.2   Natural Convection

The buoyancy effect due to density differences are included in the momentum equation for the vertical component of fluid velocity as a body force. The body force is given as the product of the Rayleigh number and the Prandtl's number.

The governing equations used for natural convection are:

$$\nabla.V = 0 \tag{2.15}$$

$$\frac{\partial u}{\partial t} + V.\nabla u = -\nabla p + Pr\nabla^2 u \tag{2.16}$$

$$\frac{\partial v}{\partial t} + V.\nabla v = -\nabla p + Pr\nabla^2 v + RaPr.T \tag{2.17}$$

$$\frac{\partial T}{\partial t} + V.\nabla T = \nabla^2 T \tag{2.18}$$

2.2   Problem Definition and Case Setup

2.2.1   Forced Convection

2.2.1.1   Computational Domain and Boundary Conditions

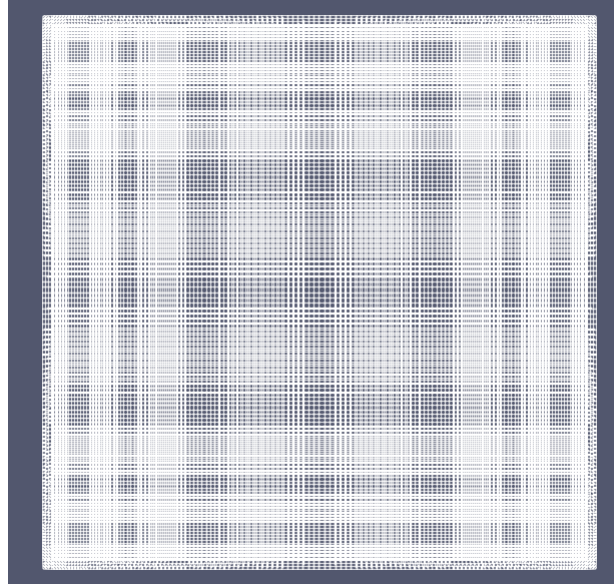A 2-D square cavity of 60x60 mesh is used as the computational grid.

Figure 2.1: Computational Grid

The two cases considered in the study for forced convection are Reynolds numbers of 100 and 1000. The velocity of the top moving wall is given as 1 m/s , the corresponding kinematic viscosity for both cases are 0.001 and 0.0001 respectively. The remaining sides are given a "noSlip" condition.The thermal diffusivity has been taken equal to the kinematic viscosity so that the Prandtl's number is equal to 1 ($\alpha = \eta$). The top wall was given a uniform temperature of 350 kelvin and the remaining walls were given 300 kelvin.

	Velocity	Pressure	Temperature(non-dimensional)
Top-Wall	(1,0,0)	zeroGradient	350
Left-Wall	noSlip	zeroGradient	300
Right-Wall	noSlip	zeroGradient	300
Bottom-Wall	noSlip	zeroGradient	zeroGradient

Figure 2.2: Boundary Conditions

2.2.1.2   Solver

The incompressible laminar solver- "icoFoam" has been modified to include the energy equation- an extra field termed "T" has been added for representing the temperature. The figure below show the energy equation added to the icoFoam solver.

```
   fvScalarMatrix TEqn
   (
       fvm::ddt(T)
     + fvm::div(phi, T)
     - fvm::laplacian(DT, T)
   );
```

Figure 2.3: Energy Equation

2.2.2   Natural Convection

2.2.2.1   Computational Domain and Boundary Conditions,

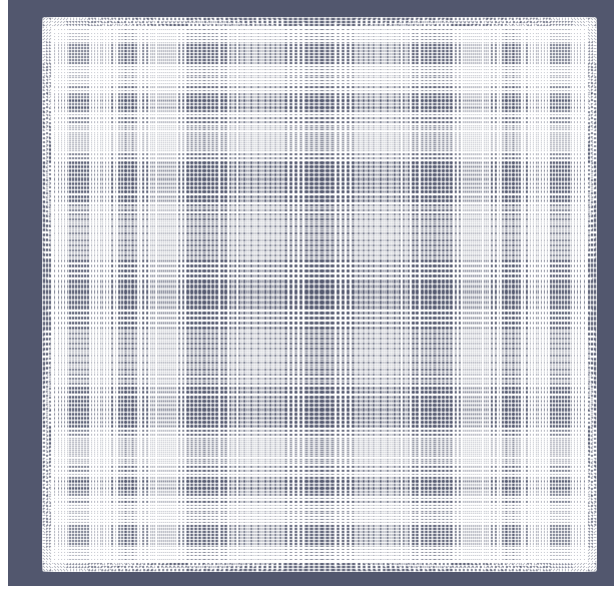The computational domain is taken as the standard square 2-D cavity. The grid consists of a 140x140 mesh.

Figure 2.4: Computational Grid

The boundary conditions are given below:

	Velocity	Pressure	Temperature(non-dimensional)
Top-Wall	(0,0,0)	zeroGradient	zeroGradient
Left-Wall	noSlip	zeroGradient	1.0(scalar)
Right-Wall	noSlip	zeroGradient	0.0(scalar)
Bottom-Wall	noSlip	zeroGradient	zeroGradient

Figure 2.5: Boundary Conditions

The Rayleigh numbers considered in this study are - 10000 (1e4) , 100000 (1e5), 1000000 (1e6)

2.2.2.2   Solver

The incompressible laminar solver -ícoFoam'is modified to include natural convection. The momentum equation is modified to include the Rayleigh number and the Prandlt number, however the symbols- β(beta) is used to account for Rayleigh Number and the symbol-g is used to account for the Prandtl number-

further the g is given as a vector- (0,Pr,0) since the buoyancy force is in the vertical direction.

The symbol DT is used for thermal diffusivity (α), since the DT is taken as equal to unity, $\eta = Pr$

```
// Momentum predictor

fvVectorMatrix UEqn
(
    fvm::ddt(U)
  + fvm::div(phi, U)
  - fvm::laplacian(nu, U)
  -beta*g*T
);
```

(a) Momentum Equation

```
fvScalarMatrix TEqn
(
    fvm::ddt(T)
  + fvm::div(phi, T)
  - fvm::laplacian(DT, T)
);
```

(b) Energy Equation

```
dimensionedScalar nu
(
    "nu",
    dimViscosity,
    transportProperties.lookup("nu")
);

dimensionedScalar DT
(
    "DT",
  //  dimViscosity,
    transportProperties.lookup("DT")
);

dimensionedScalar beta
(
    "beta",
  //  dimViscosity,
    transportProperties.lookup("beta")
);

dimensionedVector g
(
    "g",
  //  dimViscosity,
    transportProperties.lookup("g")
);
```

(c) Dimensionless Numbers used in the solver

Figure 2.6: Solver Code

2.2.3   Mixed Convection

Convection heat transfer in real life applications like car radiators are driven by a combination of forced and natural convection. The solver and grid are identical to the natural convection case however, the top moving wall is given an imposed velocity resulting in shear-driven and buoyancy-driven flow. Furthermore the top wall is given a dimensionless temperature of 1.0 and bottom wall is given that of 0.0.

|	Velocity	Pressure	Temperature(non-dimensional)
Top-Wall	(Uo,0,0)	zeroGradient	1.0(scalar)
Left-Wall	noSlip	zeroGradient	zeroGradient
Right-Wall	noSlip	zeroGradient	zeroGradient
Bottom-Wall	noSlip	zeroGradient	0.0(scalar)

Figure 2.7: Boundary Conditions

## 2.3   Results and Discussion

2.3.1   Forced Convection

The Reynolds numbers included in this study are 100 and 1000. For Reynolds number equal 100, the case was run for 50 seconds at a time step of 0.0005 seconds, for the Reynolds number of 1000. the case was run for 300 seconds at the same time step. The simulation data was compared to the data published in Santos et al(2013)[5] for both cases.

The temperature along a vertical line through the middle of the cavity has been plotted as the non-dimensional quantity: $T^* = \frac{(T-300)}{(350-300)}$ along with the cavity height.
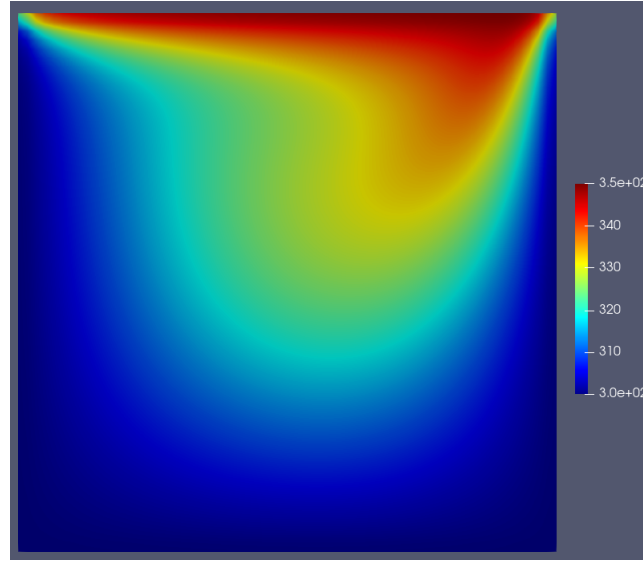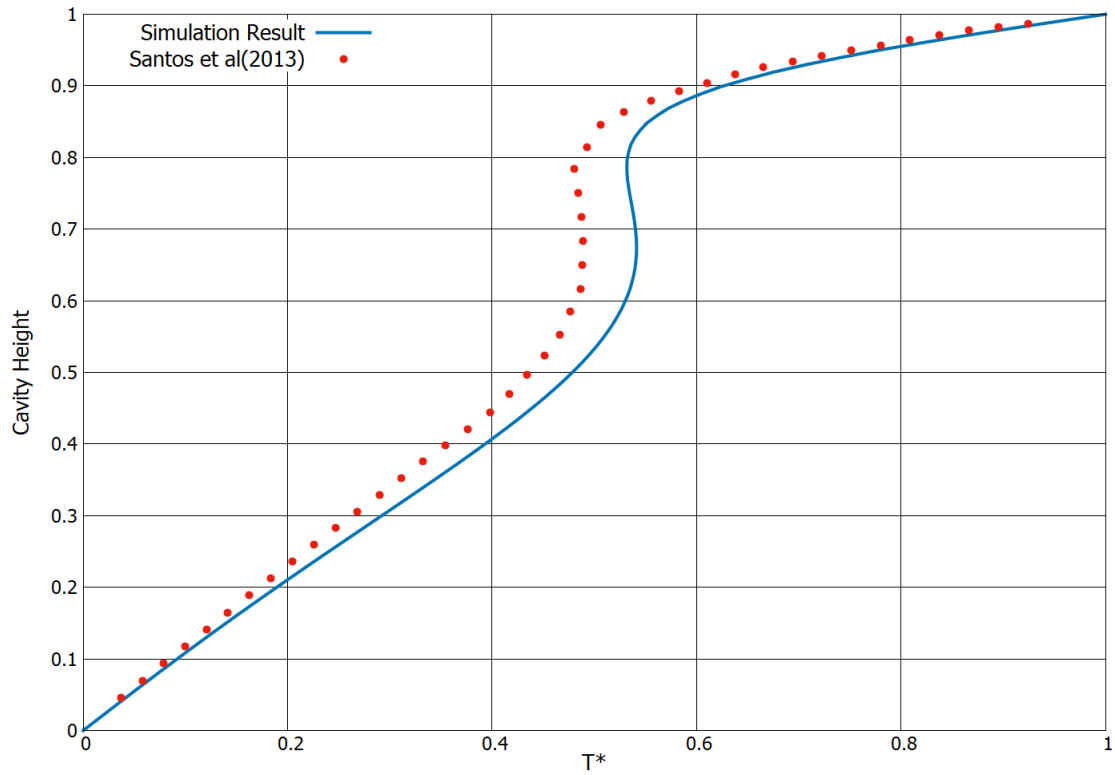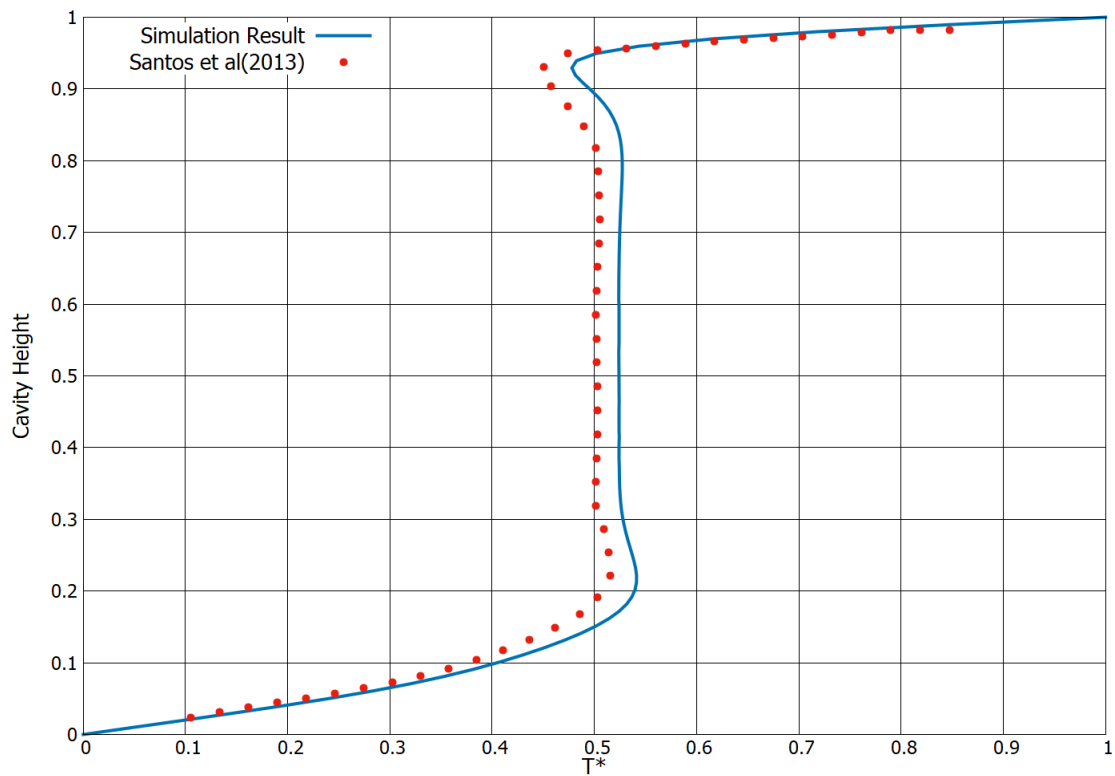

(a) Reynolds number=100
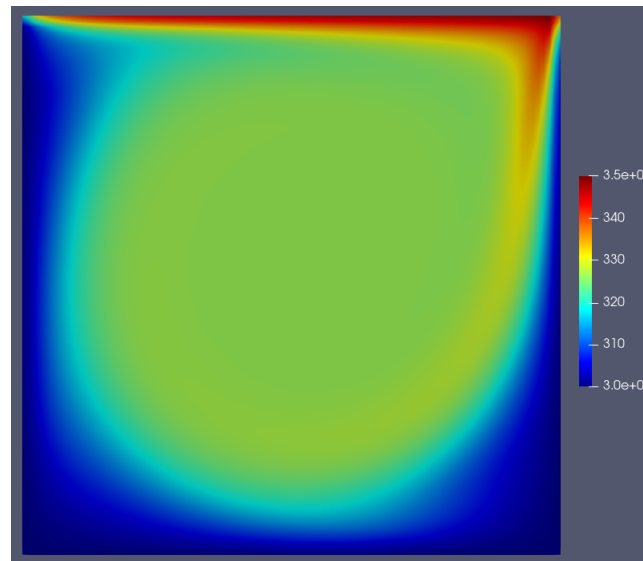
(b) Reynolds number=1000

Figure 2.8: Temperature Contour

(a) Reynolds number=100

(b) Reynolds number=1000

Figure 2.9: Comparison with Santos et al(2013)

2.3.2   Natural Convection

The four different Rayleigh numbers considered in the study- 1e4, 1e5, 1e6, the cases correspond to changes in the β(beta) in the 'transportProperties' file. After the simulation completed 120 seconds at a time step of 0.0005 seconds, the results were compared with the published data of Wan et al (2010)[19].
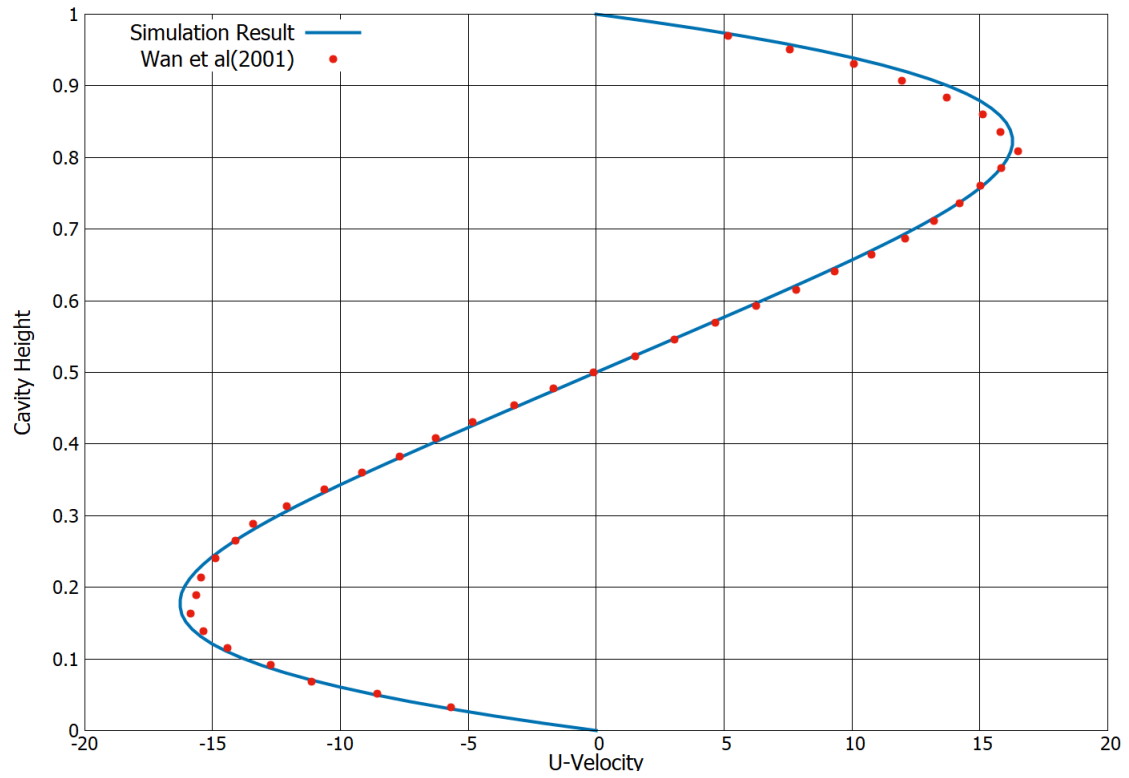
Figure 2.10: Rayleigh number=1e4
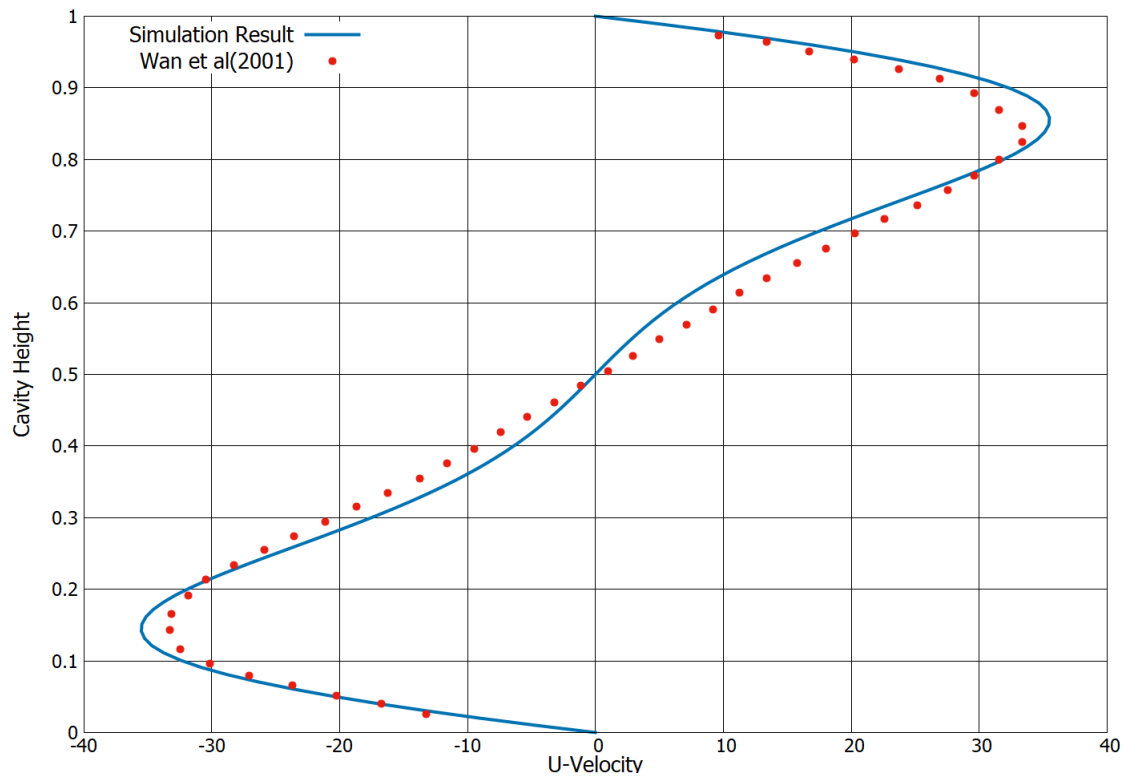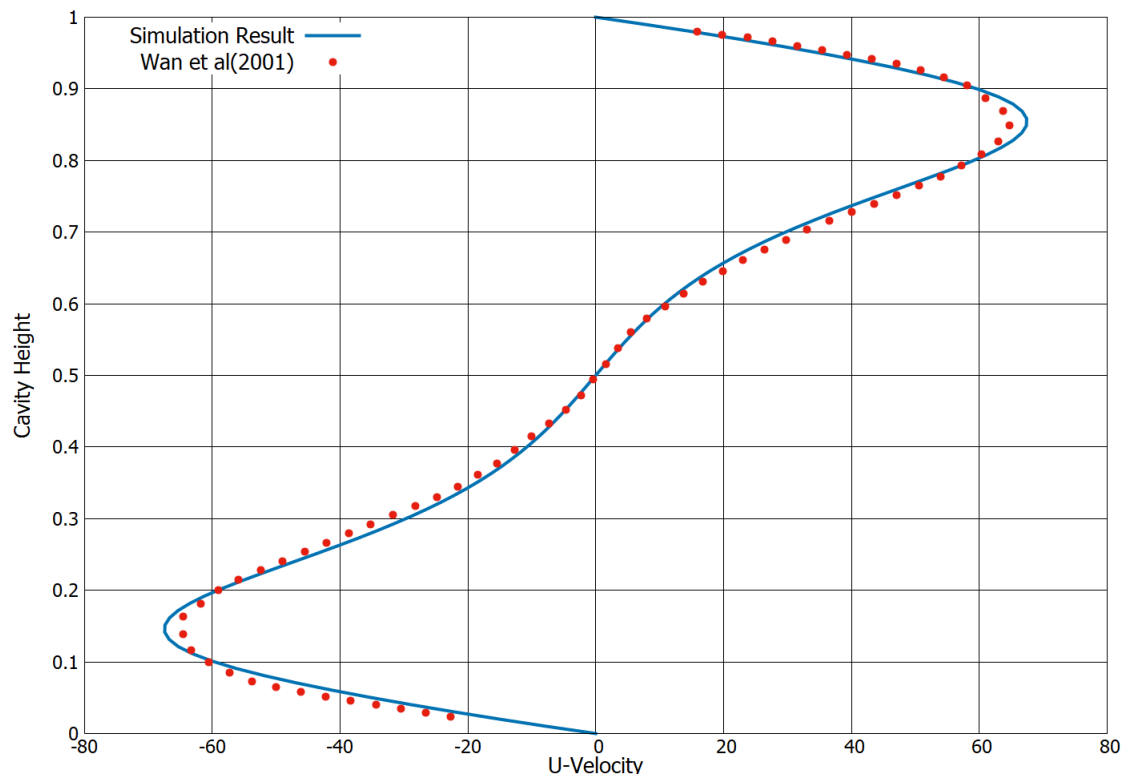

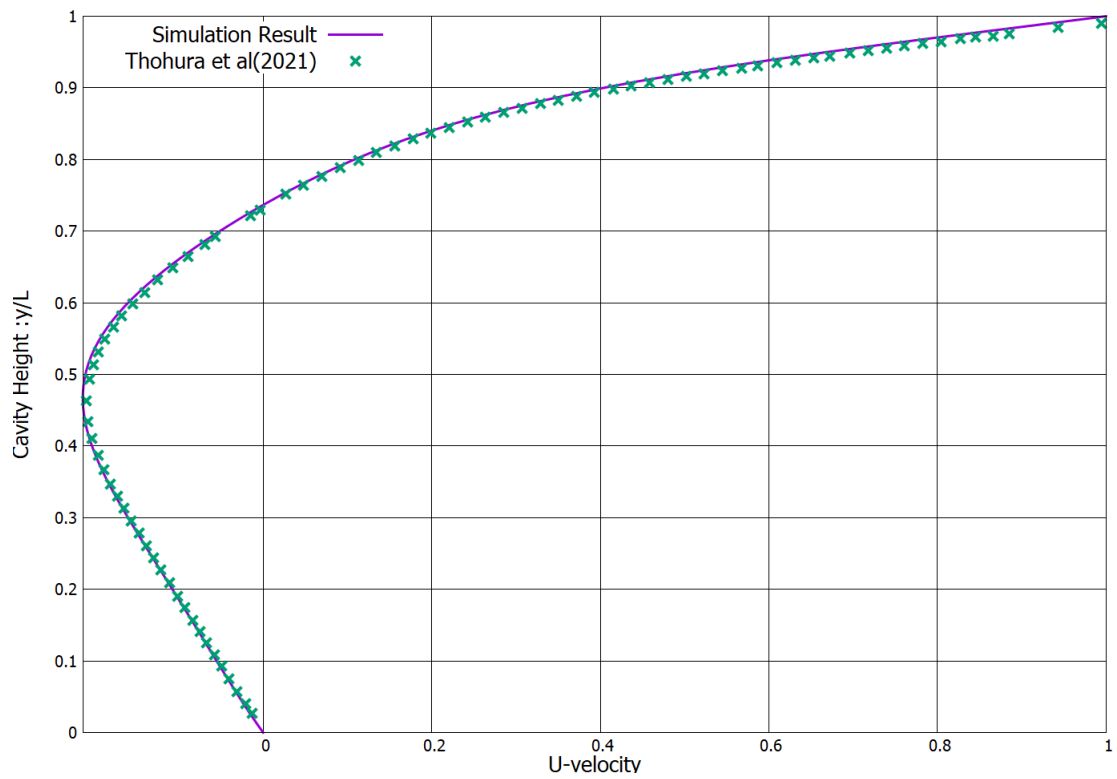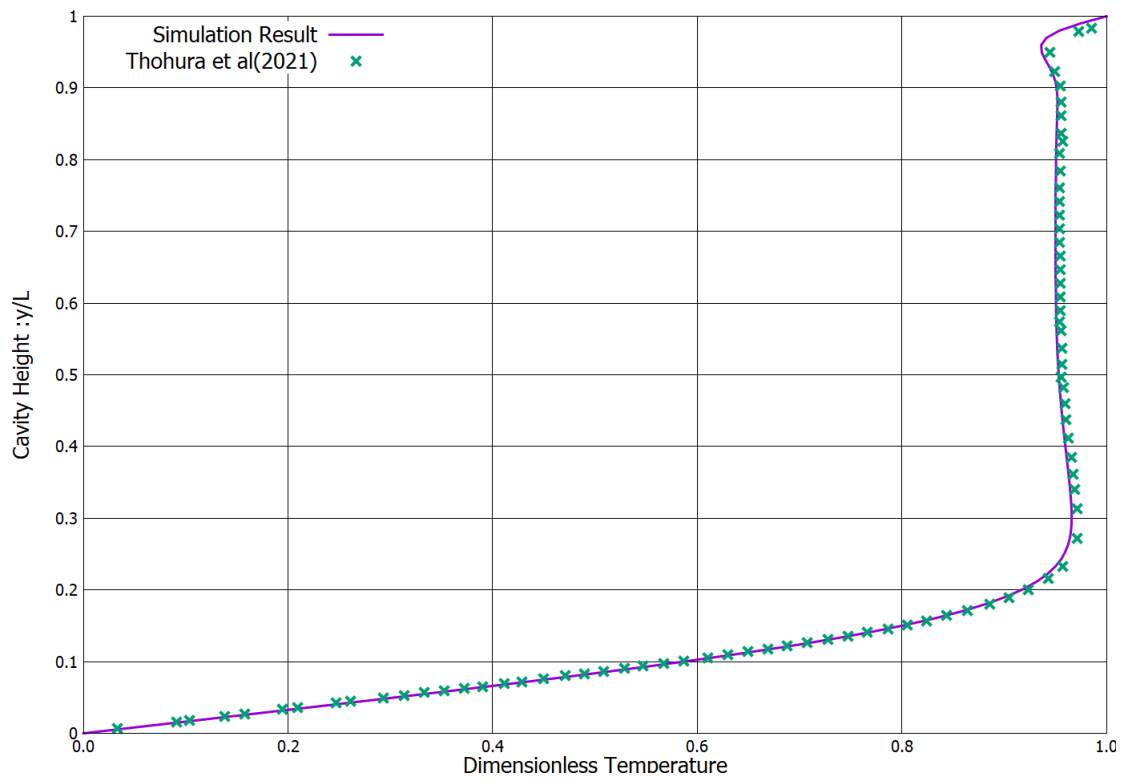
Figure 2.11: Rayleigh number=1e5

Figure 2.12: Rayleigh number=1e6

2.3.3   Mixed Convection

The cases of Richardson numbers of 0.1, 1.0 and 5.0. Results are compared to Thohura et al (2021)[18].

(a) Non-Dimensional U-velocity

(b) Non-Dimensional Temperature

Figure 2.13: Richardson Number=0.1

(a) Non-Dimensional U-velocity

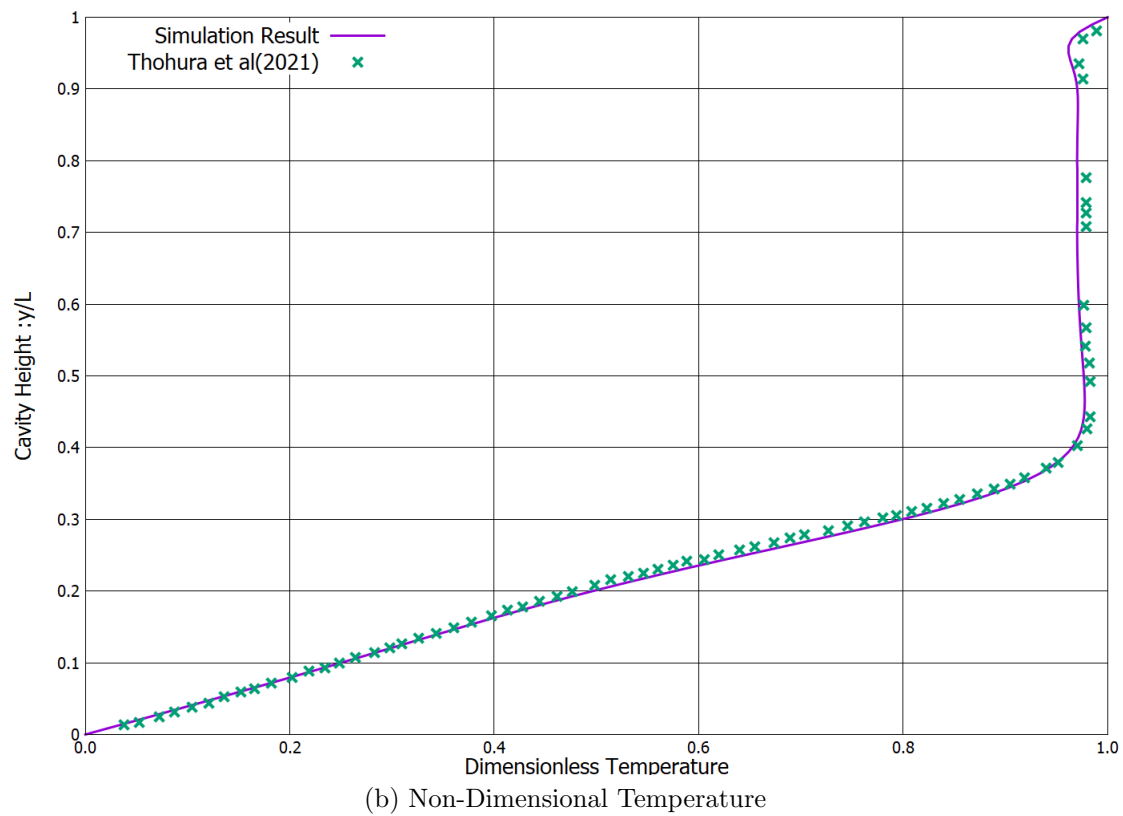

(b) Non-Dimensional Temperature

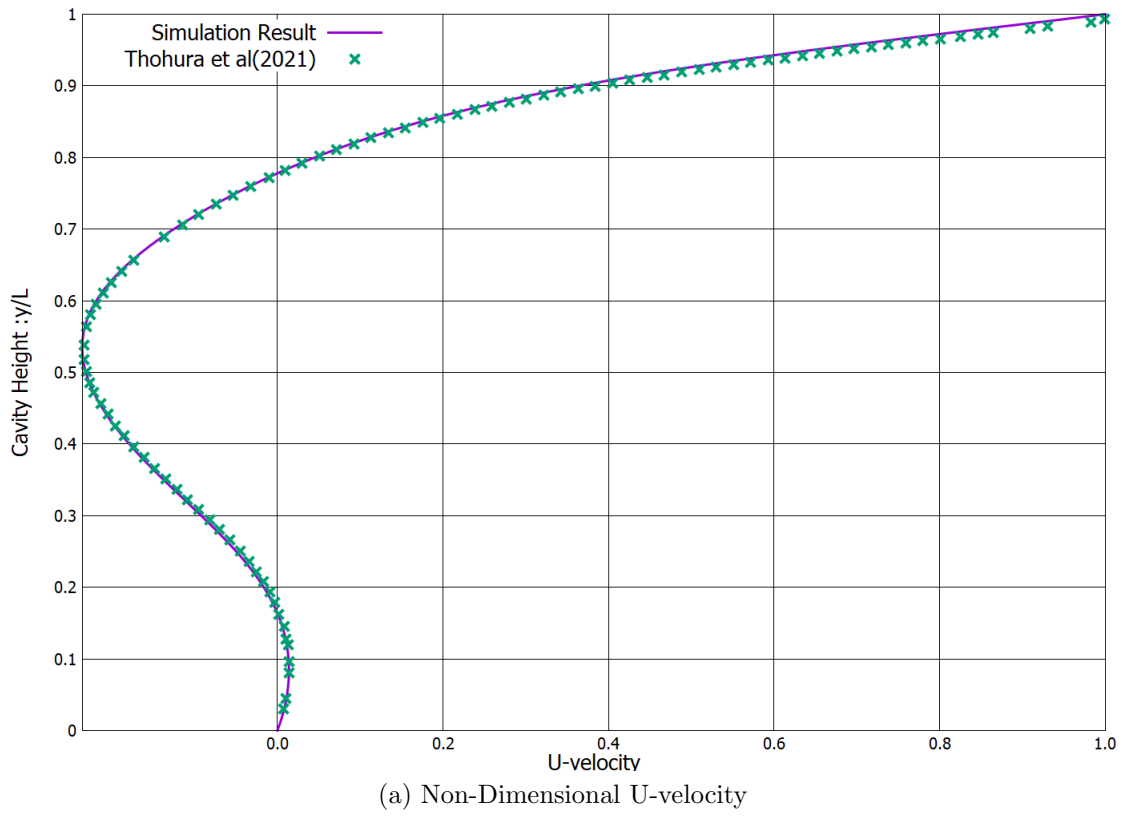Figure 2.14: Richardson Number=1
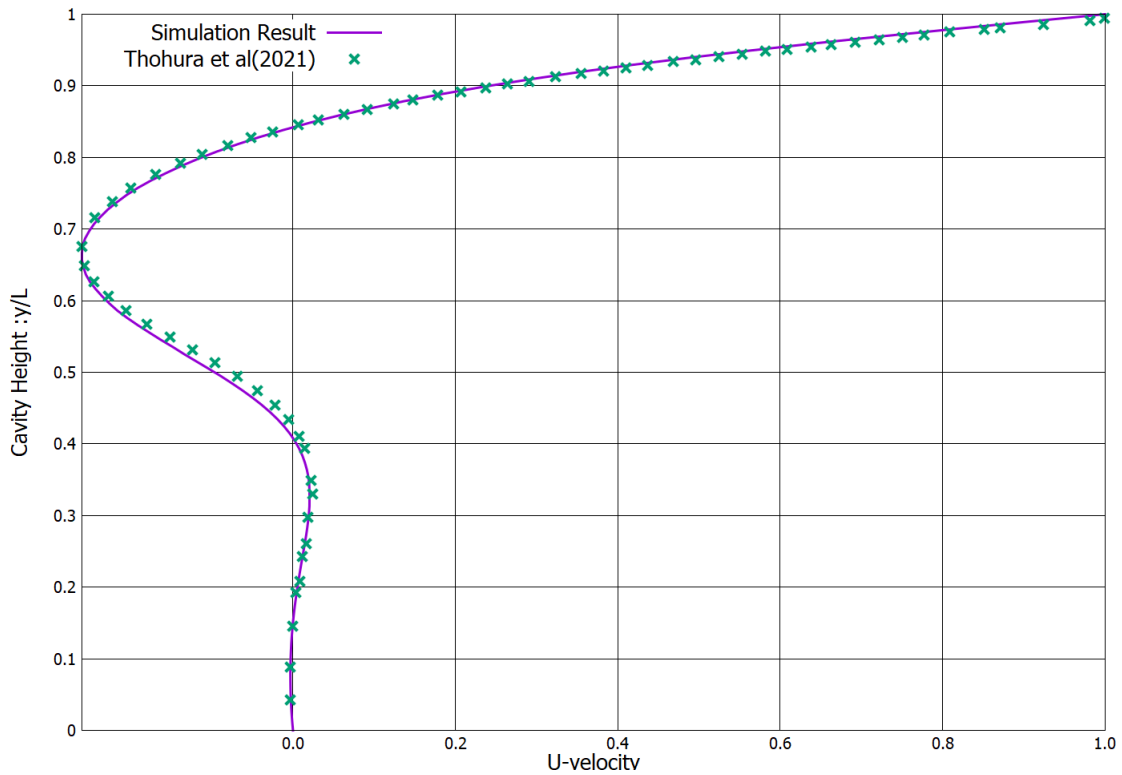
(a) Non-Dimensional U-velocity
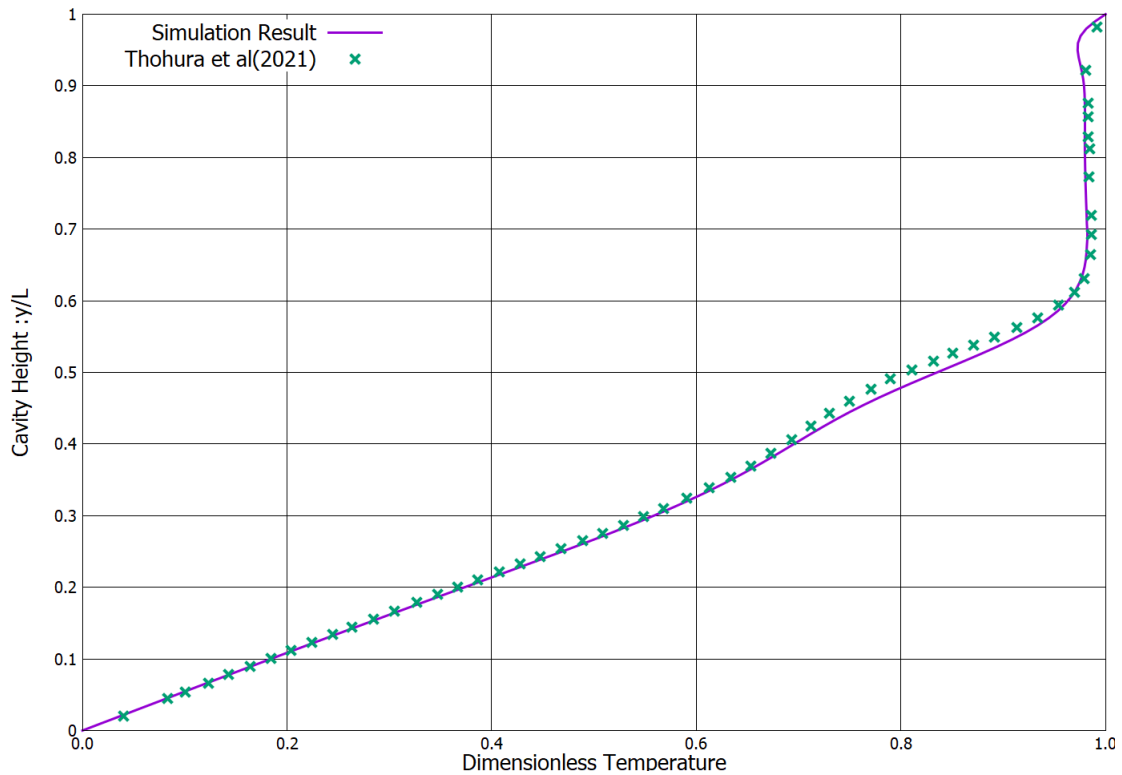
(b) Non-Dimensional Temperature

Figure 2.15: Richardson Number=5

The validation study is further extended for Iwatsu(1993) [8]. The results are presented for Grashof number of 1e6 and Reynolds numbers of 100, 400, 1000 and 3000 with the Prandtl number as 0.71.

Figure 2.16: Reynolds Number =100

Figure 2.17: Reynolds Number =400

Figure 2.18: Reynolds Number =1000

Figure 2.19: Reynolds Number =3000

Turbulence modelling for Magnetohydrodynamics and Mixed convection flow

Turbulence modelling for Magnetohydrodynamics and Mixed convection flow

3.1 Introduction

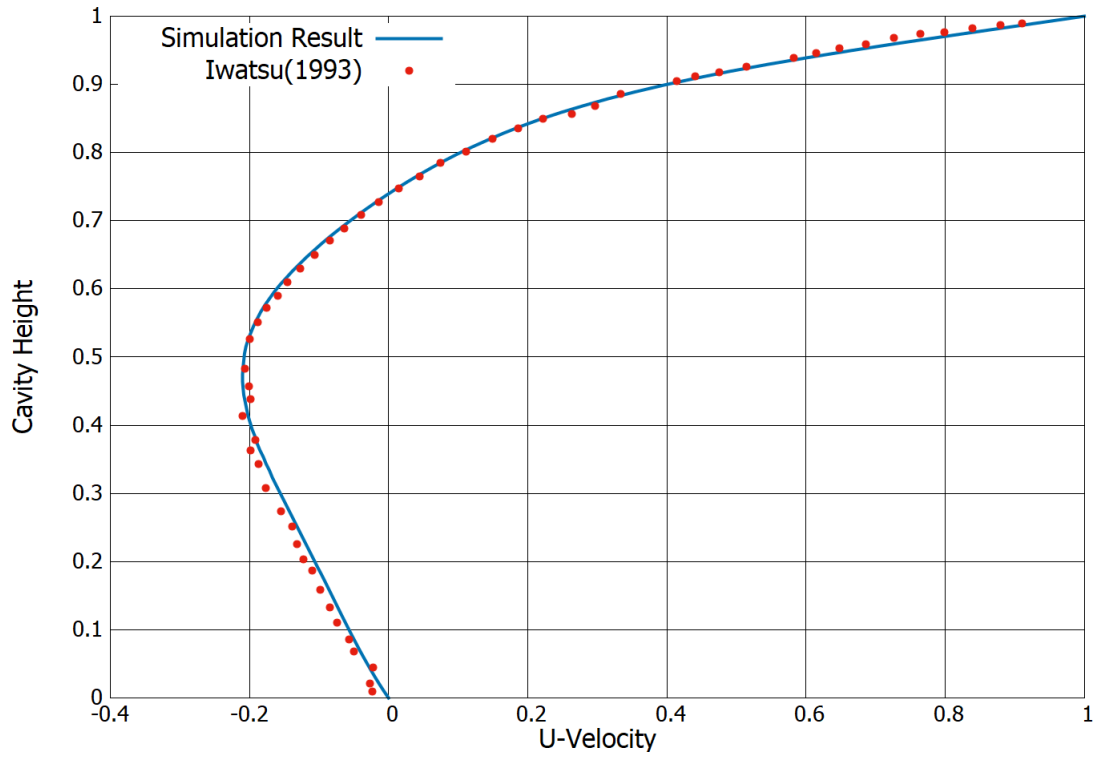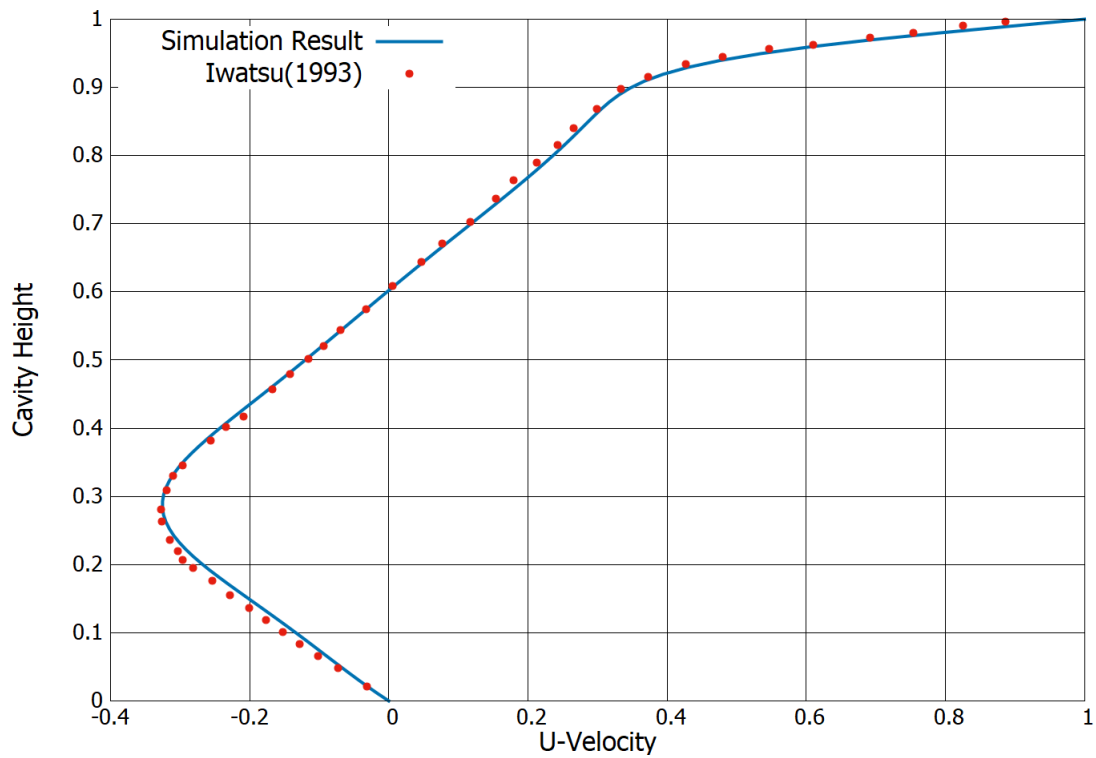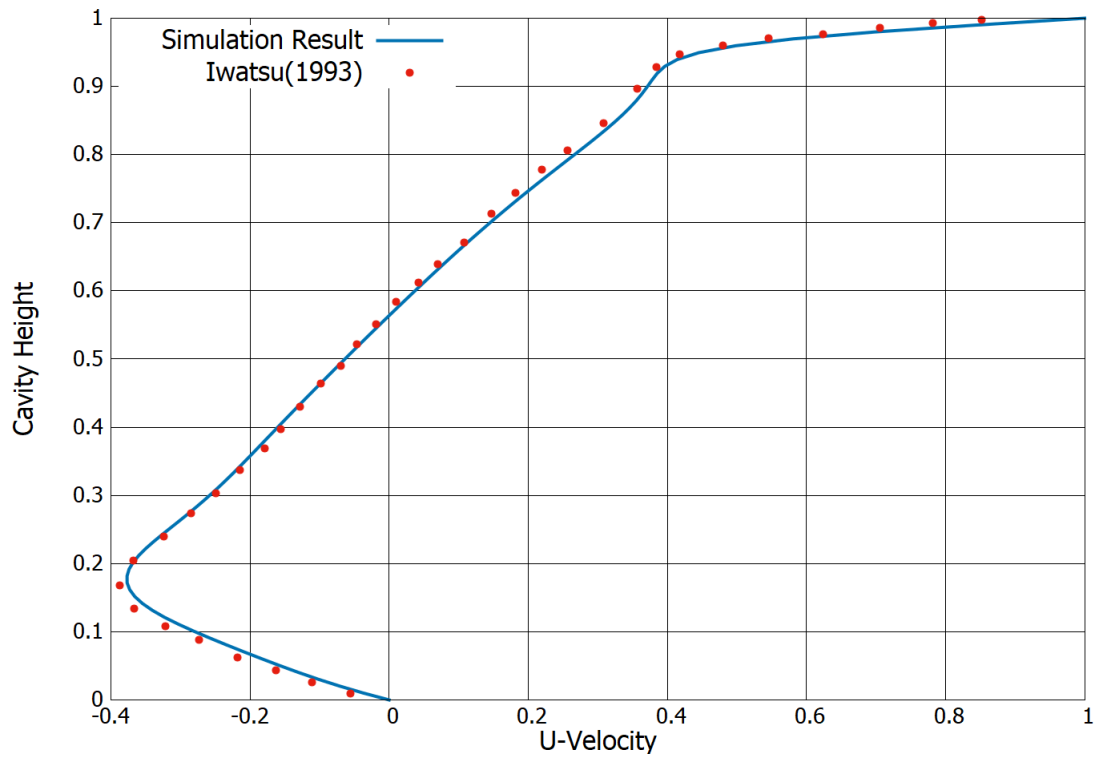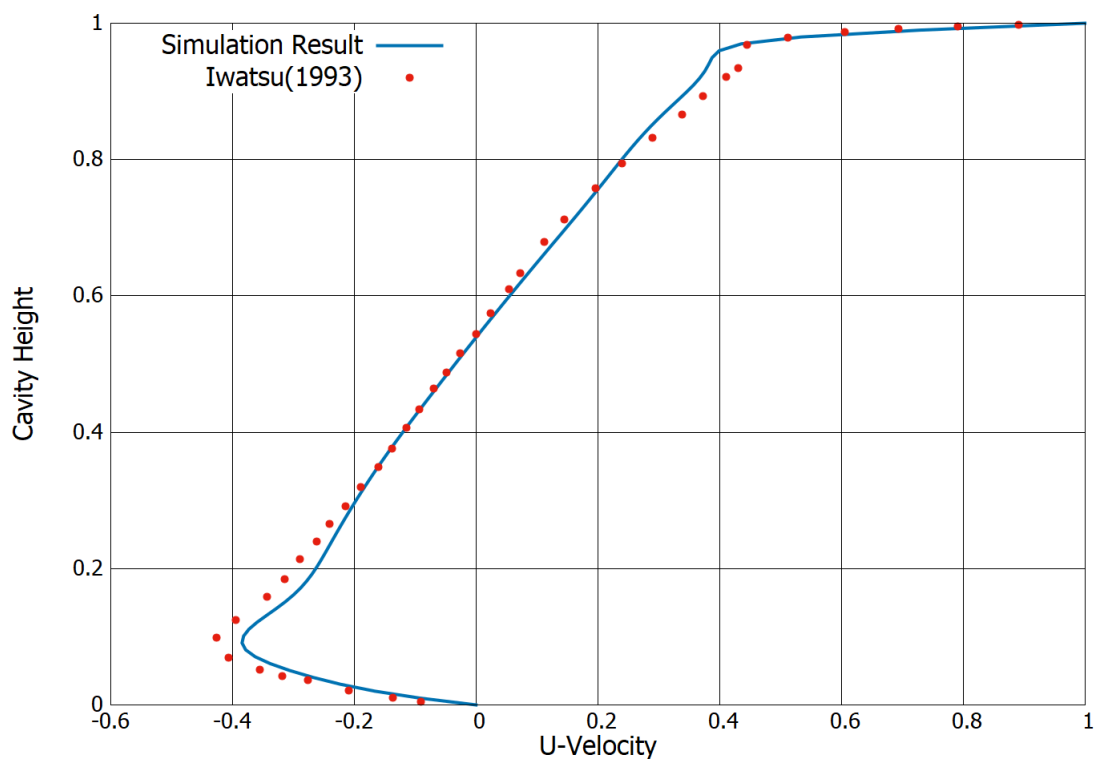The study has been extended to include the high Reynolds number flows of both magnetohydrodynamics and mixed convection. For the high Reynolds numbers, turbulence models are utilized to account for the turbulent behaviour of the fluid. The study is conducted by creating a new OpenFOAM solver which combines both Lorentz force and buoyancy force (modelled using the Boussinesq approximation) in the Navier-Stokes equation. The K-Epsilon turbulence model is used which is a standard OpenFOAM turbulence model for the Reynolds-Averaged Navier-Stokes equation (RAS) .The solver is tested in three stages of validation - the first is for pure turbulent fluid flow with Chen&Jaw(insert citation) , next turbulent natural convection with Markatos(insert citation) and pure MHD with Kefayati(2014) [9] .

3.1.1 K-Epsilon turbulence model

The Reynolds approach to modelling turbulence is to split the three velocity components into a steady term and a fluctuating term(Eq. 3.1). The steady component is the time-averaged component and the time averaging of the fluctuating component is assumed to be equal to zero.

$$U = \overline{U} + U' \tag{3.1}$$

This results in the Reynolds-Averaged Navier Stokes equation (RAS) (written in

compressible form) in Eqn 3.2

$$\frac{\partial(\rho U)}{\partial t} + \nabla.(\rho UU) = -\nabla p + \nabla.[\mu(\nabla U + (\nabla U)^T)] + \rho g - \nabla(\frac{2}{3}\mu(\nabla.U)) - \nabla.(\rho\overline{U'U'})$$
(3.2)

The final term is the Reynolds Stress which is the divergence of the product of the two fluctuation velocity components which have been averaged. The K-Epsilon model computes the mean velocity components and in order to do so the Reynolds stress term needs to be modelled.

The Boussinesq hypothesis calculates the Reynolds stress using the gradients of the mean velocity components and turbulent viscosity(μ_t). Therefore the K-Epsilon model is one approach to calculate the turbulent viscosity to close the equations. The turbulent viscosity is calculated algebraically (Eqs .3.3 and 3.5) using the turbulent kinetic energy (k) and turbulent dissipation rate (ϵ). Therefore a transport equation (Eq. 3.4) is solved to compute the two quantities.

$$\mu_t = C_\mu \frac{\rho k^2}{\epsilon}$$
(3.3)

$$\frac{\partial(\rho k)}{\partial t} + \nabla.(\rho U k) = \nabla.[(\mu + \frac{\mu_t}{\sigma_k})\nabla k] + Sources + Sinks$$
(3.4)

$$\frac{\partial(\rho\epsilon)}{\partial t} + \nabla.(\rho U \epsilon) = \nabla.[(\mu + \frac{\mu_t}{\sigma_\epsilon})\nabla\epsilon] + Sources + Sinks$$
(3.5)

Five model coefficients are used for the $k - \epsilon$ model. The values used in standard OpenFOAM solver are:

Constant	Value
C_μ	0.09
C1	1.44
C2	1.92
C3	0.0
σ_k	1.0
σ_ϵ	1.3

Figure 3.1: Turbulence model constants

3.1.2   Turbulent Heat Transfer

The thermal diffusivity for turbulent flow is computed by adding a second component to the laminar thermal diffusivity (Eq .3.6). This component is the ratio of the turbulent viscosity and the turbulent Prandtl number.

$$\alpha_{effective} = \alpha_{Laminar} + \frac{\mu_t}{Pr_t} \qquad (3.6)$$

where ,

μ_t - Turbulent Viscosity

Pr_t - Turbulent Prandtl number (0.9 for air).

The non-dimensional heat transfer coefficient "Nusselt Number" is also included in the validation and analysis.

3.1.3   Solver

A steady state solver is created which computes the mean velocity components along with the magnetic field and temperature field. Two extra forces - Lorentz force and Buoyancy force are added to the momentum equations. The Boussinesq hypothesis is further utilized for computing the buoyancy force. A separate post-processing code was used for computing the Nusselt number and wall heat flux.

3.2   Case Setup

The $k - \epsilon$ model in OpenFOAM requires the values of k,ϵ and μ_t to be supplied as boundary conditions. These values are computed using the constants using the following equations based on initial velocity.

$$k = \frac{3}{2}(U_{ref} * I)^2 \qquad (3.7)$$

$$\epsilon = \frac{C_\mu^{0.75} * k^{1.5}}{l} \qquad (3.8)$$

$$\mu_t = C_\mu \frac{k^2}{\epsilon} \qquad (3.9)$$

where ,

I:- turbulence intensity

U_{ref}:- Lid Velocity

l :- length of lid * turbulence intensity

3.3   Validation

3.3.1   Fluid Flow

The turbulent fluid flow with no external magnetic field and buoyancy force is analysed for a cubic cavity with a 30x30x30 grid. Results for Reynolds number of 3200 and 10000 are compared with Prasad and Koseff(1989)[14]. The lid velocity has been taken as 1 m/s and the standard wall functions are used for k, ϵ and μ_t.

Boundary Conditions :

1. Top Wall : U -(1 0 0) , T-

2. Botttom Wall : U = noSlip

3. Left Wall : U = noSlip
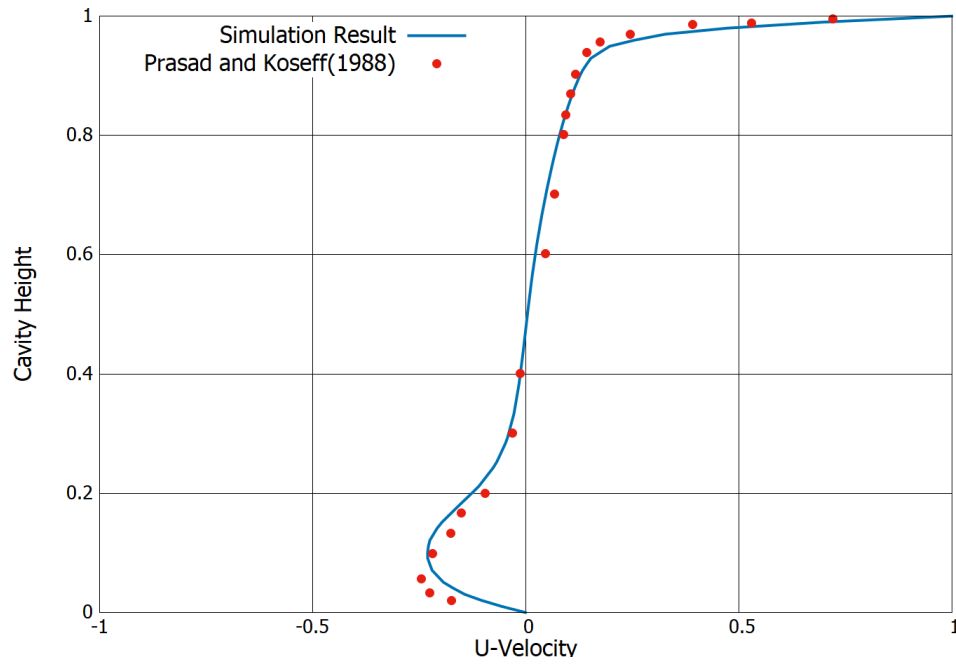
(a) Comparison of U-Velocity along the vertical mid of the XY Plane
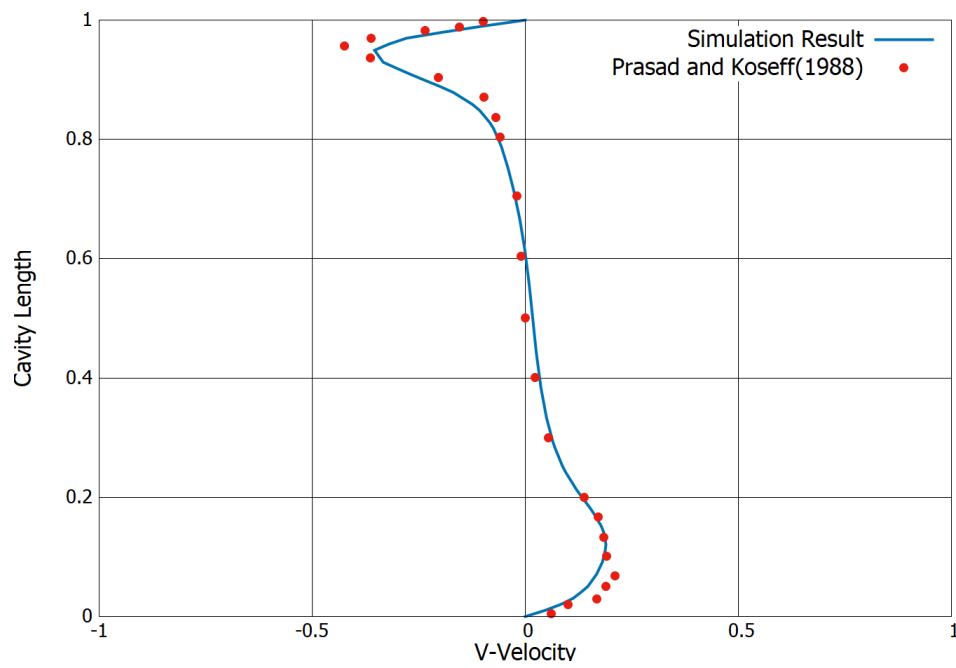
(b) Comparison of U-Velocity along the vertical mid of the XY Plane

Figure 3.2: Reynolds Number =3200
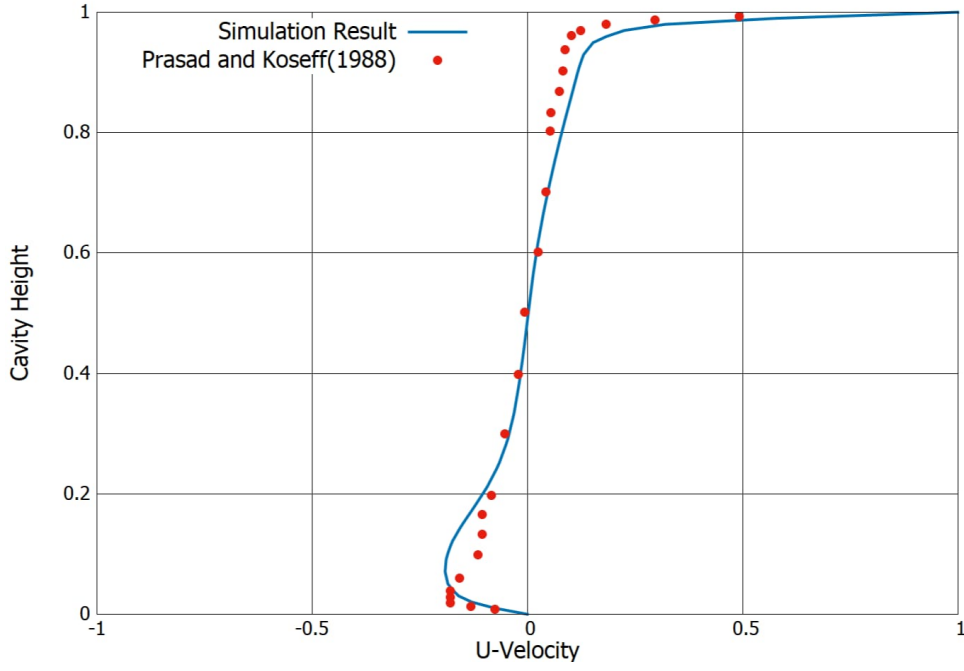
(a) Comparison of U-Velocity along the vertical mid of the XY Plane
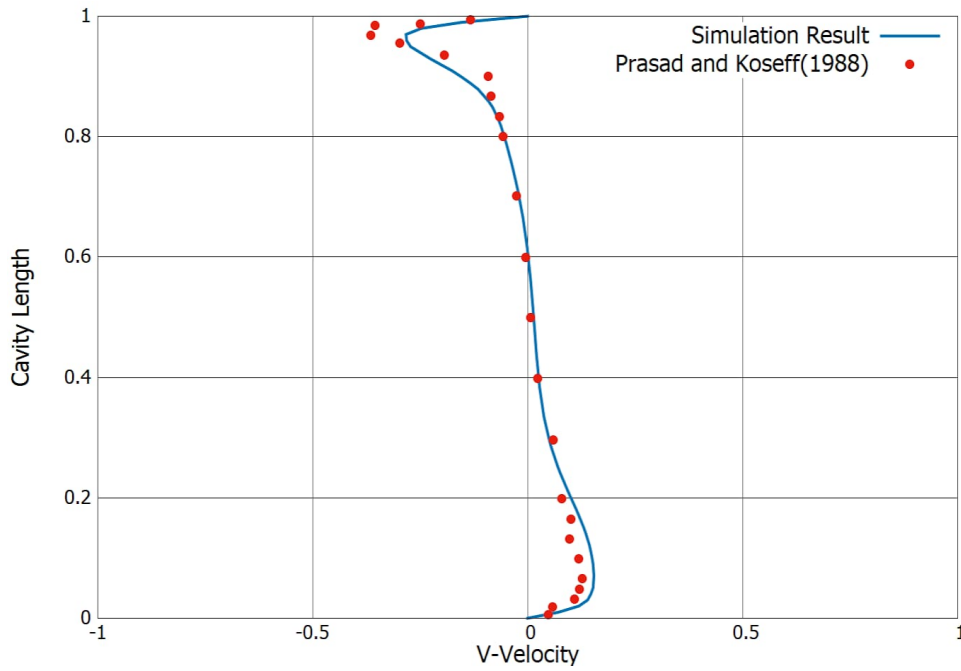
(b) Comparison of U-Velocity along the vertical mid of the XY Plane

Figure 3.3: Reynolds Number =10000

3.3.2   Turbulent Heat Transfer

The validation of the natural convection flow with $k - \varepsilon$ model was done using Markatos(1984)[10]. The turbulent cases are considered for Rayleigh numbers of 1e6 and greater. The top velocity is given as zero since the case is for natural convection, however the U_{ref} is computed as given below and is used in Eqns 3.7,3.8,3.9

to compute the initial values of the three turbulent variables.

$$U_{ref} = \sqrt{(g\beta\triangle TH)} = \sqrt{\frac{Ra * nu * nu}{Pr}} \tag{3.10}$$

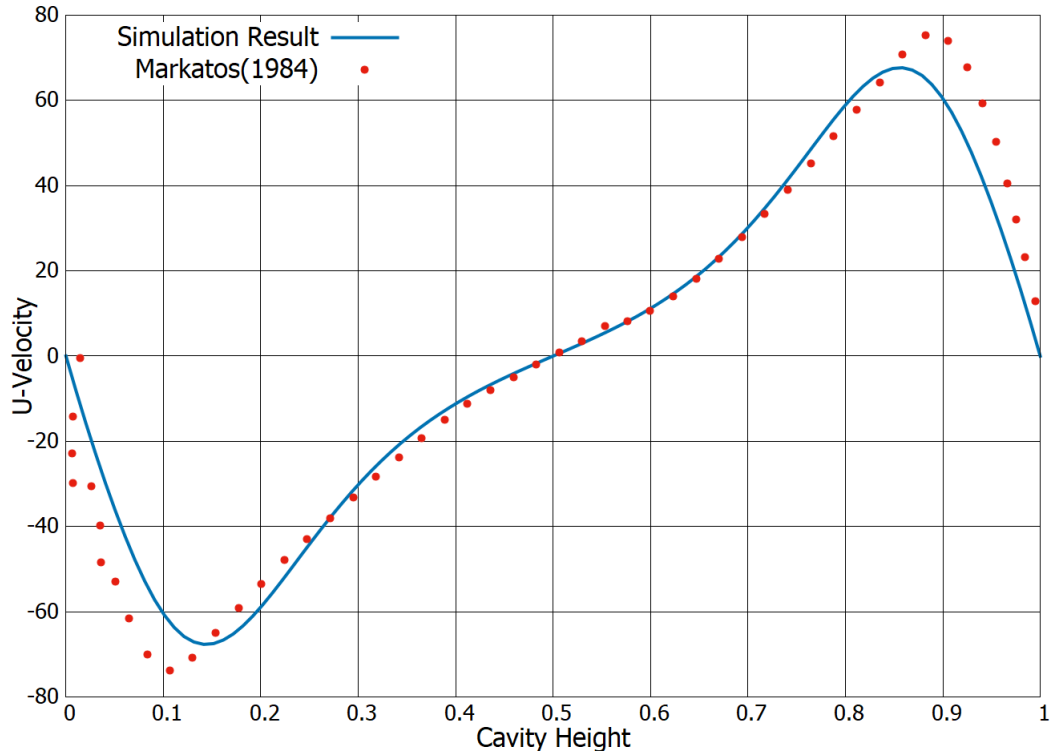The initial validation study consisted of a velocity comparison for Rayleigh number of 1e6.

Figure 3.4: Comparison of U-Velocity along the vertical mid-line of the cavity
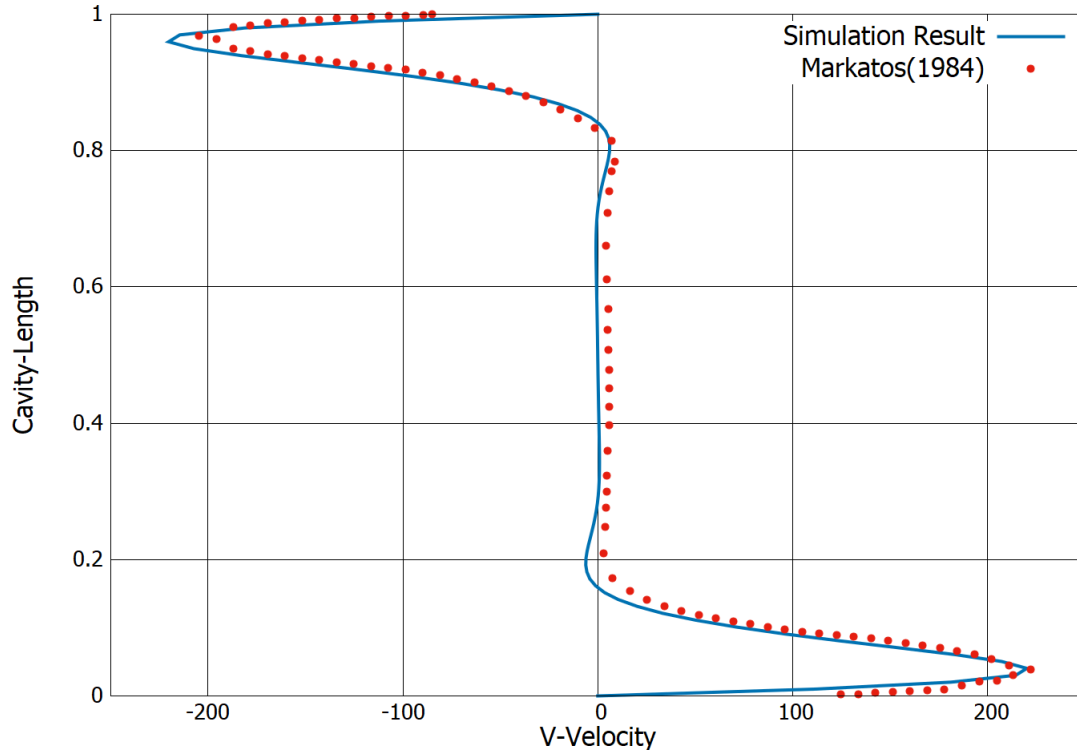
Figure 3.5: Comparison of V-Velocity along the horizontal mid-line of the cavity

The validation is extended for Rayleigh numbers of 1e6,1e8,1e10 and consists of the maximum of U-velocity along the vertical mid-line and the maximum value of V-velocity along the horizontal mid-line.

	Rayleigh Number	1e6	1e8	1e10
Vmax along y=0.5	Simulation	220.247	2118.08	17492.0
	Markatos(1984)	221.8	1812	16890
Umax along y=0.5	Simulation	67.673	513.359	2950.94
	Markatos(1984)	68.81	514.3	2323

Figure 3.6: Comparison with Markatos(1984)

The non-dimensional Nusselt number is computed at the left wall (hot wall) using the wall-heat flux which is in-turn computed using wall functions available in OpenFOAM. The Nusselt number is computed using the formula(Eqn.3.11)

$$Nu(y) = (\frac{\dot{q}_{wall}}{\alpha C_p \rho}) * (\frac{D}{T_H - T_C}) \qquad (3.11)$$

where,

$\dot{q}_{wall}$ - Wall Heat Flux

α- Thermal Diffusivity

C_p- Specific Heat Capacity of air (1005 J/g/K)

D - Length of the cavity

T_H, T_C- Hot and cold wall temperatures

	Rayleigh Number	1e6	1e8	1e10
Nu_{max}	Simulation Result	17.7414	85.86843	376.8212
	Markatos(1984)	17.872	61.06	361.47
Nu_{avg}	Simulation Result	8.9833	35.0473	160.1477
	Markatos(1984)	8.754	32.045	156.85
Nu_{min}	Simulation Result	1.1172	3.52825	16.7126
	Markatos(1984)	1.232	5.2246	23.462

Figure 3.7: Comparison of Nusselt Number with Markatos(1984)

3.3.3   Magnetohydrodynamics

The new steady state solver is tests for its MHD performance with published data in Kefayati(2014)[9]. Due to the unavailability of turbulent MHD data, the turbulence in the solver was turned off. This section of validation is to test the working of the steady state MHD solver . The Hartmann number is considered in this case are two extreme values of 10 and 100 are used in conjunction with Reynolds numbers of 100 and 1000.
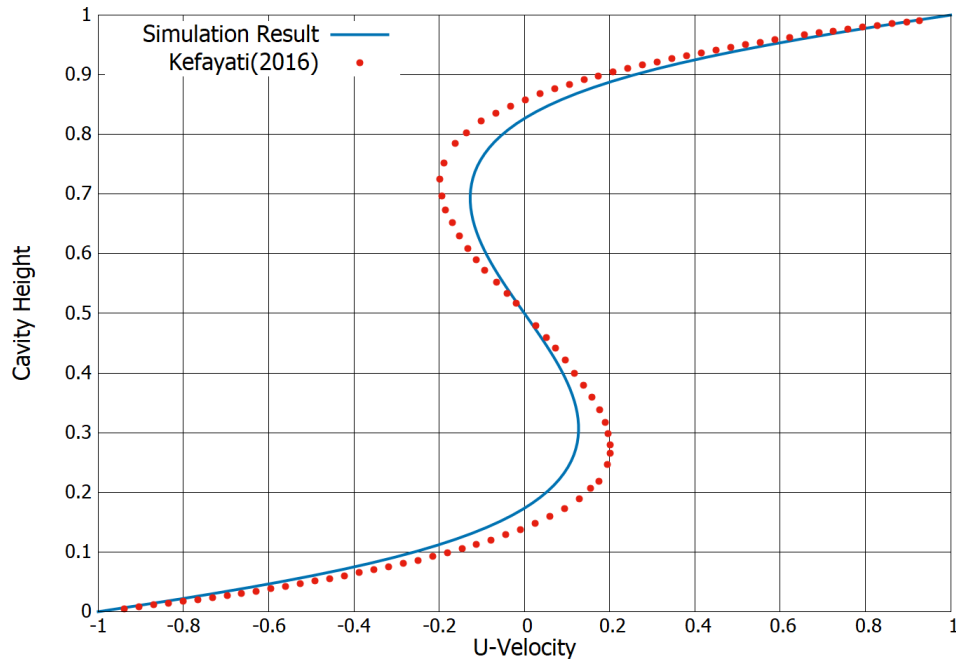

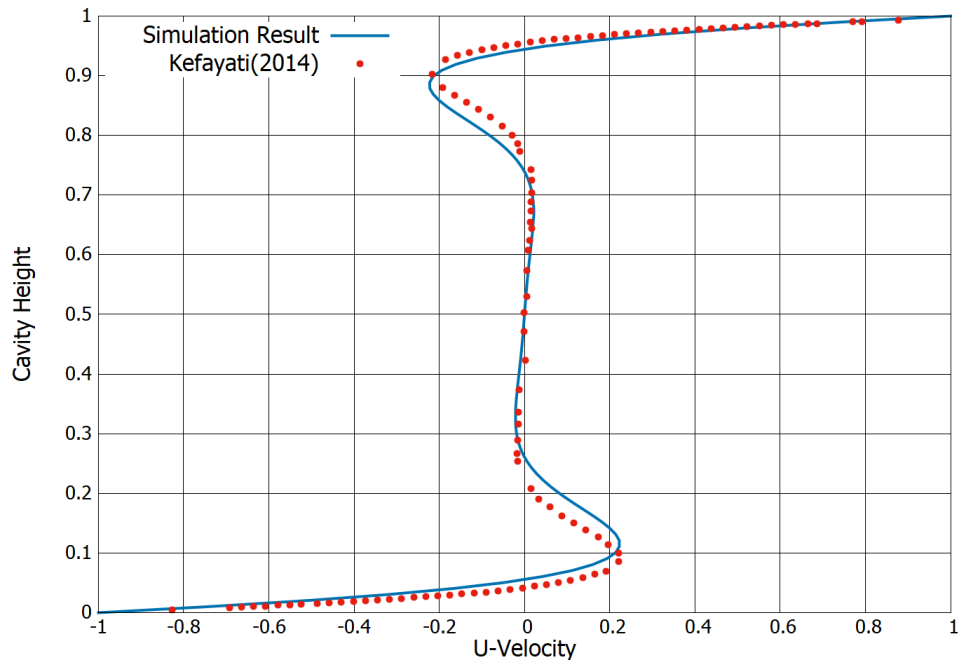Figure 3.8: Reynolds Number=100, Hartmann Number =10

Figure 3.9: Reynolds Number=1000, Hartmann Number =100

Bibliography

[1] T. Cheng. Characteristics of mixed convection heat transfer in a lid-driven square cavity with various richardson and prandtl numbers. *International Journal of Thermal Sciences*, 50(2):197–205, 2011.

[2] T. Chiang and T. W. H. Sheu. A numerical revisit of backward-facing step flow problem. *Physics of Fluids*, 11(4):862–874, 1999.

[3] A. Cortes and J. Miller. Numerical experiments with the lid driven cavity flow problem. *Computers & Fluids*, 23(8):1005–1027, 1994.

[4] I. Demirdžić, Ž. Lilek, and M. Perić. Fluid flow and heat transfer test problems for non-orthogonal grids: bench-mark solutions. *International Journal for Numerical Methods in Fluids*, 15(3):329–354, 1992.

[5] E. D. dos Santos, A. P. P. an L. A. O. Rocha, and F. H. R. Franca. Numerical study of forced convection lid-driven cavity flows using LES (Large Eddy Simulation). *Journal of Energy and Power Engineering*, 7:1669–1680, 2013.

[6] L. Fuchs and N. Tillmark. Numerical and experimental study of driven flow in a polar cavity. *International Journal for numerical Methods in Fluids*, 5(4):311–329, 1985.

[7] U. Ghia, K. N. Ghia, and C. T. Shin. High-Re solutions for incompressible flow using the Navier-Stokes equations and a multigrid method. 48:387–411, 1982.

[8] R. Iwatsu, J. M. Hyun, and K. Kuwahara. Mixed convection in a driven cavity with a stable vertical temperature gradient. *International Journal of Heat and Mass Transfer*, 36(6):1601–1608, 1993.

[9] G. R. Kefayati. FDLBM simulation of magnetic field effect on non-Newtonian blood flow in a cavity driven by the motion of two facing lids. *Powder Technology*, 253:325 – 337, 2014.

[10] N. C. Markatos and K. Pericleous. Laminar and turbulent natural convection in an enclosed cavity. *International journal of heat and mass transfer*, 27(5):755–772, 1984.

[11] V. Martin, A. Drochon, O. Fokapu, and J.-F. Gerbeau. MagnetoHemoDynamics in the aorta and electrocardiograms. *Physics in Medicine and Biology*, 57(10):3177–3195, may 2012.

[12] M. Moallemi and K. Jang. Prandtl number effects on laminar mixed convection heat transfer in a lid-driven cavity. *International Journal of Heat and Mass Transfer*, 35(8):1881–1892, 1992.

[13] N. Ouertatani, N. B. Cheikh, B. B. Beya, T. Lili, and A. Campo. Mixed convection in a double lid-driven cubic cavity. *International Journal of Thermal Sciences*, 48(7):1265–1272, 2009.

[14] A. K. Prasad and J. R. Koseff. Reynolds number and end-wall effects on a lid-driven cavity flow. *Physics of Fluids A: Fluid Dynamics*, 1(2):208–218, 1989.

[15] F. Selimefendigil and A. J. Chamkha. Magnetohydrodynamics mixed convection in a lid-driven cavity having a corrugated bottom wall and filled with a non-newtonian power-law fluid under the influence of an inclined magnetic field. *Journal of Thermal Science and Engineering Applications*, 8(2), 2016.

[16] M. Taher, H. Kim, and Y. Lee. High prandtl number mixed convection cavity flow using lattice boltzmann method. *European Scientific Journal*, 9(33), 2013.

[17] F. Talebi, A. H. Mahmoudi, and M. Shahi. Numerical study of mixed convection flows in a square lid-driven cavity utilizing nanofluid. *International Communications in Heat and Mass Transfer*, 37(1):79–90, 2010.

[18] S. Thohura, M. M. Molla, M. A. Sarker, and M. C. Paul. Study of mixed convection flow of power-law fluids in a skewed lid-driven cavity. *Heat Transfer*, 2021.

[19] D. C. Wan, B. S. V. Patnaik, and G. W. Wei. A new benchmark quality solution for the buoyancy-driven cavity by discrete singular convolution. *Numerical Heat Transfer, Part B: Fundamentals*, 40(3):199–228, 2001.